Comparison of UAV-based LiDAR and Photogrammetry Case Study: Litchfield SuperSite, Australia

Tobias Klapper
UU: 6188397
t.klapper@students.uu.nl
Geographical Information Management and Applications
Faculty of Geoinformation and Remote Sensing
Wageningen University & Research
Supervisor: Dr. HM Bartholomeus

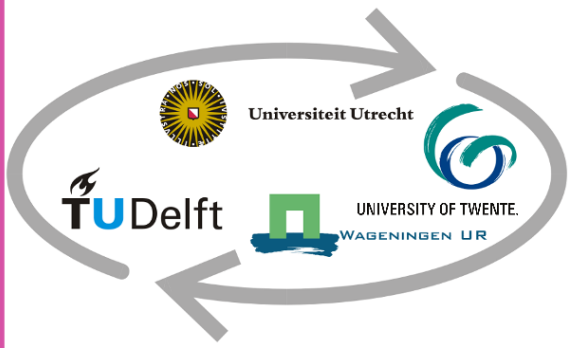

Acknowledgments

This thesis was written in order to fulfil the course requirements of the MSc. programme Geographical Information Management and Applications (GIMA).

I would like to give special thanks to my supervisor Dr. Harm Bartholomeus from Wageningen University & Research, who was supportive throughout this challenging research process. Further, I want to thank my family, friends and fellow GIMA students for their support and motivation, and always giving me valuable feedback and advice during this time.

Tobias Klapper
Utrecht, 25th of February 2020

Abstract

In the last decade Light Detection and Ranging (LiDAR) and structure-for-motion (SfM) photogrammetry became the two leading techniques for gathering 3D point cloud data. Especially combined with an Unmanned Aerial Vehicle (UAV) these two techniques have shown to be useful for environmental studies or forestry. The low costs for UAV-based SfM photogrammetry is one of the main advantages of this technique. LiDAR on the other hand has the advantage that it allows to map the ground even with vegetation cover.

This research aims to determine to which point structure-for-motion photogrammetry can be used as a replacement to LiDAR in savanna ecosystems. This is done in the first step by comparing Digital Terrain Model (DTM), Digital Surface Model (DSM), and Canopy Height Model (CHM). In the second step forest parameters, as tree count, Diameter at Breast Height (DBH), canopy area in m^2, gap area in m^2, are being compared.

It was found that the photogrammetric derived digital models can be used as an alternative to the LiDAR derived models and further it can be used as an alternative for estimating most of the forest parameters. The DBH could not be calculated for a single tree in either of the two datasets, when the results of the tree segmentation are used.

Table of Contents

List of Figures

List of Tables

List of abbreviations

CHM	Canopy Height Model
CSF	Cloth Simulation Filter
DEM	Digital Elevation Model
DTM	Digital Terrain Model
DSM	Digital Surface Model
LiDAR	Light Detection and Ranging
PCA	Principal Component Analysis
SfM	Structure for Motion
UAV	Unmanned Aerial Vehicle

1. Introduction

1.1. Study Area

1.1.1. Importance of Savanna ecosystems

Savannas are in areas with certain characteristics as rainfall ranges between 50-130 cm per year, average temperature above 20°C. Further, savannas are the ecosystems which occur between tropical rainforest and grasslands. The most distinctive feature of savannah ecosystems compared to forests or grasslands is the co-domination of trees and grasses, which means that there is a heterogeneity in the vegetation cover and in more detail that there is an intermittent tree canopy with scattered areas of grasses and bare soil in between. Further characteristic for savannas is the existence of a dry and a rain-season, the dry season has a duration of at least a month. Also, regular fires are typical for savannas and have a major impact of the spatial pattern of tree-grass cover. The main limiting factor for the vegetation cover is the soil moisture as it is the main water source in the dry periods for the plants (Ford *et al.*, 2016).

Savannas are important because they cover a fifth of the earth land surface (Sankaran *et al.*, 2005) and further they play an important role in the global carbon circle as approximately 30% of the global carbon store in terrestrial ecosystems is stored in savannas (Chen *et al.*, 2003). Savannas can function as carbon sinks, because they are rich in biodiversity and are able store a lot of carbon in woody biomass and the soil. The problem for their function in the carbon circle is that they undergo a rapid land use change especially in warm biomes as in Africa (Gwenzi and Lefsky, 2014).

Further, it is important to monitor savannas because they support a large amount of the world's population, which is also still rapidly growing (Bodini and Clerici, 2016). According to (Sivkumar, 2007) up to 33% of the world's population, is depending on functioning savanna ecosystems for grazing their livestock, and removal of trees as building material and as firewood. But due to the increasing population this also leads to disturbances and land degradation (Alam and Starr, 2013).

For the savanna ecosystems there are three threats, which are climate change, bush encroachment, and agricultural conversion (Southworth *et al.*, 2016).

Therefore, it is important to monitor structure and height of the savanna woodland for a better understanding of the role in the global carbon cycle and further for monitoring the biodiversity. Monitoring the extent of savannas is also important for tracking desertification, especially in

Africa and to monitor the endangerment of the ecosystem by land use change and agricultural conversion.

To monitor savannas different parameters, as canopy cover to estimate the biomass in these ecosystems. For calculating these parameter different intermediate models are needed, such as digital elevation models (DEM). DEMs are spatial distribution of elevation for a specific area and is a general term for depicting a spatial pattern of any surface. In this research both types of DEM are going to be analyzed. The first type of a digital elevation model is a digital terrain model (DTM) which is firmly limited to the Earth's bare terrain (Gupta, 2018).

The other type of DEM is the digital surface model (DSM), which contains in contrast to the DTM also objects on the ground such as trees, bridges, and buildings. These two distinct types of DEM are needed to construct a canopy height model (CHM). A CHM represents the absolute height distribution of vegetation canopy above the terrain and it can have a high influence on extracted forest inventory information (Chen *et al.*, 2018). Because of the importance of CHM for forestry it is used for the comparison between the two remote sensing techniques.

Forest parameters are key values in this research as well as key figures in the description of a savanna ecosystem, which main characteristic is the continuous herbaceous layer of grasses and sedges and a discontinuous layer of trees (Skarpe, 1992). Therefore, the forest parameters as tree count, canopy cover, and the respective area of bare ground are going to be calculated. Further the diameter at breast height (DBH) is going to examined which is parameter which is required for modern forestry (Fritz *et al.*, 2013).

1.1.2. Study Area

The study area is the Litchfield Savanna SuperSite in the Litchfield National Park, near Darwin in the Northern Territories of Australia. A SuperSite is defined as an intensive ecosystem observatory of one of the ecosystems occurring in Australia and have the scale of 10 – 200 km^2. The Litchfield Savanna SuperSite is a typical tropical savanna woodland area, which means it is a frequently burnt, high rainfall, savanna, with an area of 5x5 km, which corresponds to the extent of vegetation cover required for satellite-based remote sensing, and is located in the Litchfield National Park (TERN, no date). The Litchfield Savanna SuperSite was set up to be able to answer research questions regarding the impacts of prevailing fire regimes on vegetation structure and composition, the influence of vegetation structure, climate drivers, and fire regimes on savanna carbon sequestration (Karan *et al.*, 2016).

Figure 1: Location of the SuperSites (Karan *et al.*, 2016)

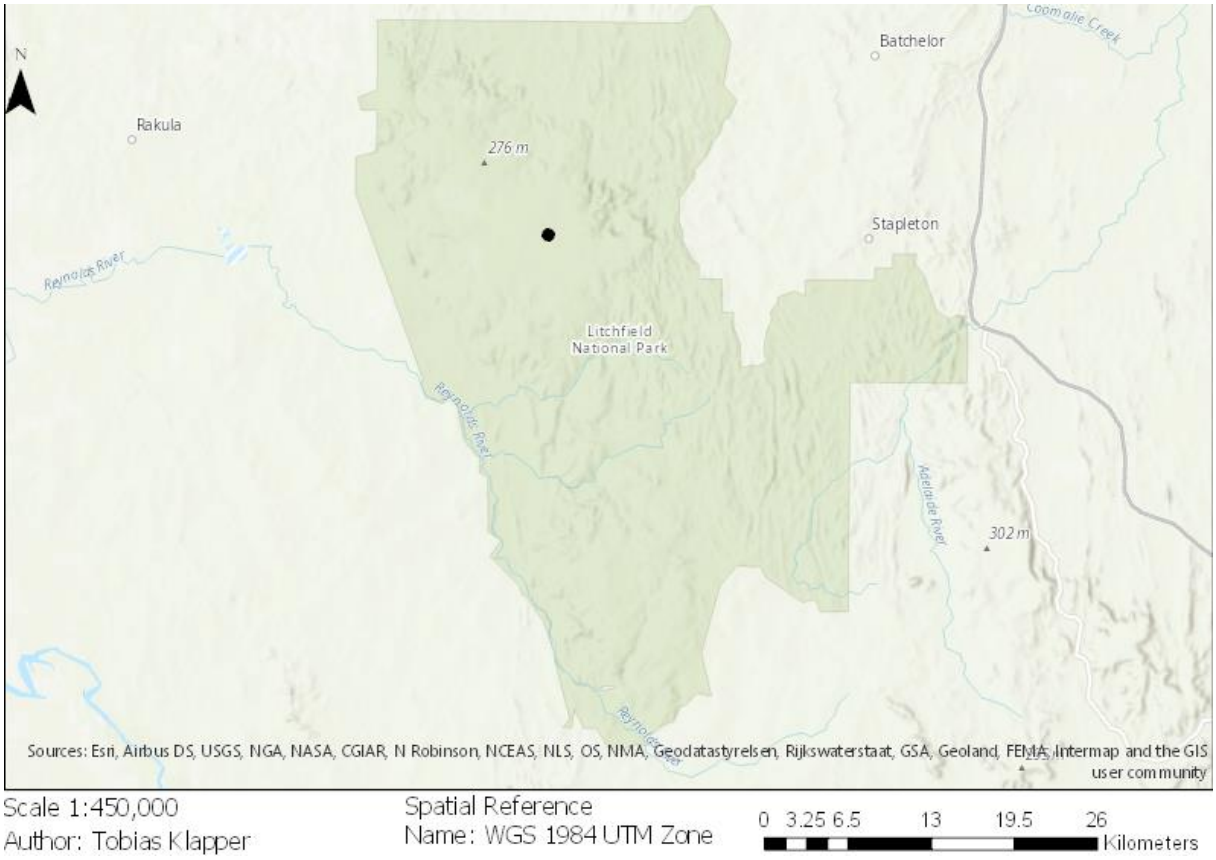

Figure 2 Location of the study area in the Litchfield National park

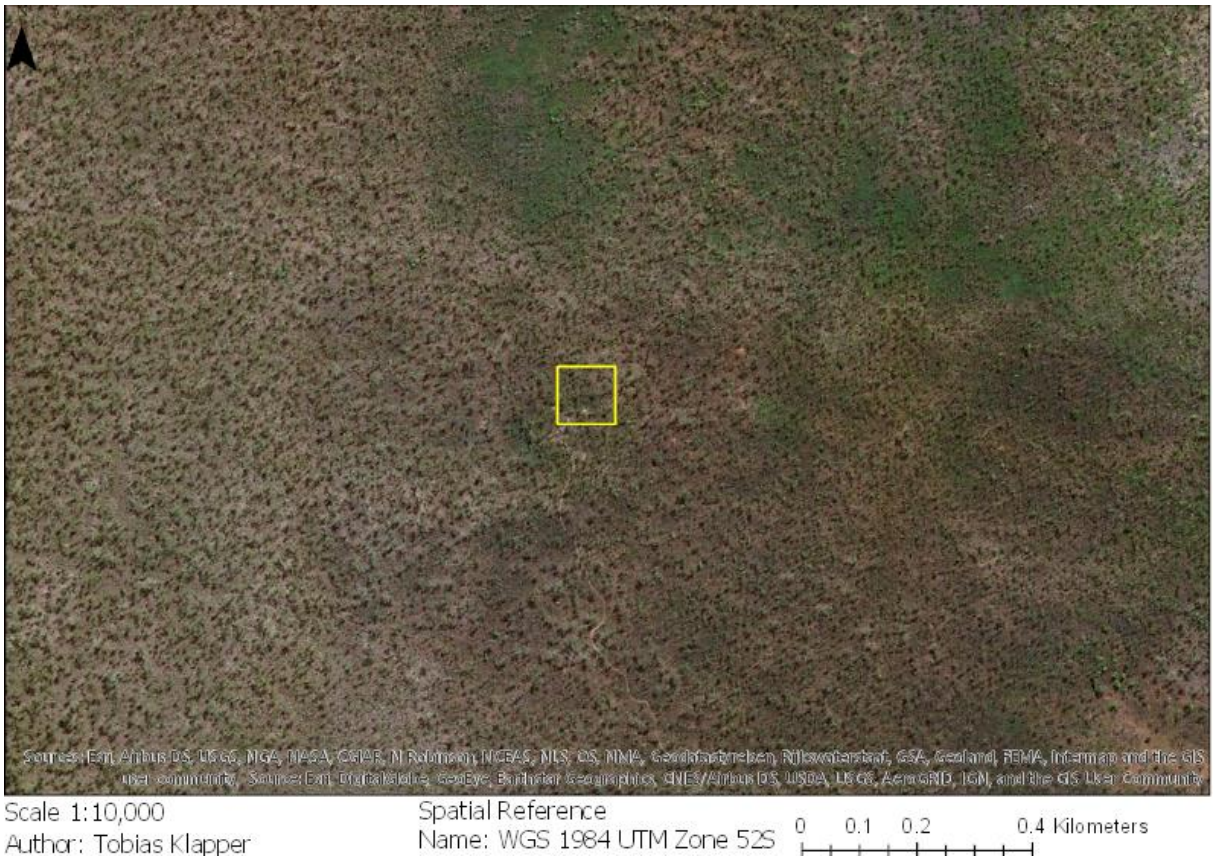

Figure 3 Aerial photograph of the study area

1.2. Technical Background

1.2.1. Unmanned Aerial Vehicle

Unmanned aerial vehicle (UAV) can be defined as an aircraft without a human pilot aboard, where a flight can be remotely controlled, fully or intermittently autonomously controlled by onboard computers. The term UAV is often used in legislation whereas the term drone has the same definition but is not used in legislation. Therefore it is the most common used term to describe UAVs (Awange, 2018).

The development of UAVs was driven by the military and was first mainly amalgamated as aircrafts without pilots. Until the year 1990 UAVs were mainly developed and used for military purposes. From the start of the 1990's on UAVs became more and more interesting for civil applications as well. Most aircrafts were developed for environmental measurements (Awange, 2018).

The main components, which almost all UAVs, consist of are the unmanned aircraft, the ground control station, and the data link. The unmanned aircraft is the main component and defines different classifications of drones. Drones can be classified by two criteria, first based on flight

platforms and second based on size and weight. The classification based on weight and size is used for the legislation regarding UAVs and therefore are varying for every country. The UAVs which are of interest for this research can be classified as Low Altitude, Short-Endurance (LASE), and have characteristics as a wingspan lower than 3 m, flight times around 2 hours and flight ranges limited to a few km. Nowadays the main functions of the ground control station are the remote control, real-time data display and data exchange relay. The last important component is the data link system, which is keeping the communication between the UAV and the ground control station, and is in control of controlling, tracking, locating, and the data transmission of the UAV and its sensors (Awange, 2018).

1.2.2. LiDAR technology

LiDAR is an acronym for laser imagining detection and ranging or light detection and ranging. The first endeavors in the field of LiDAR were made in the 1930s when the determination of the scattering intensity of search beams was used to measure atmospheric characteristics like air density (Wandinger, 2005). The first systems were developed between the 1960s (Lemmens, 2011a) and the early 1970s (Ackermann, 1999) in the United States and Canada. The next step towards airborne and therefore UAV-based LiDAR systems was the development of global positioning system (GPS) which was the solution for the critical positioning problem because it made high accuracy positioning possible (Ackermann, 1999). The development of the systems was technology driven. The main advantage which drove the development is that LiDAR allows to map the ground even if the area is covered by vegetation. This is possible through the recording of first and last parts of backscattered laser pulses. Further, LiDAR has the advantage that weather conditions have only marginal influence on the flights and therefore LiDAR data collection is independent of the weather condition and daytime (Lemmens, 2011a). The main components of a LiDAR system are a laser scanner, a global positioning system and internal navigation system. The laser scanner measures the distance between the sensor and the surface by computing the time delay between the emission of the laser impulse and the detection of the returning impulse. The laser scanner has two main components, the transmitter and the receiver. The transmitter emits short light pulses with lengths between a few and several nanoseconds depending on the laser. Further most transmitters are equipped with a beam expander, which decreases the divergence of the laser pulses before they leave the transmitter unit. The receiver component of the laser scanner contains three parts: a telescope which detects the backscattered parts of the pulses, an optical analyzer which selects specific polarizations

and wavelengths required by the following detector. The wavelength and polarization depend on the system used. Afterwards the remaining light pulses are forwarded to a detector where the optical signal are converted into electrical signal (Wandinger, 2005).

1.2.3. Photogrammetry

Photogrammetry is about measuring in photos by using the overlapping areas of the photographs. These photos are obtained by cameras mounted on satellites, aircrafts, or UAVs. The first use of photogrammetry in the United States was in 1862 by the Union Army (Lemmens, 2011b). The further development of photogrammetry is closely bound to the progresses in camera and aviation development. Specific cameras were developed for taking aerial photographs, because for high quality results it is a necessity to have high precision optics and mechanics. Important for these systems is good lens correction, large film formats and a high stability to deliver the needed parameters for the following calculations. Due to technological improvements in the field of photography and in high-detail consumer cameras, these cameras have reached sufficient geometric resolution and technical standards, that these cameras can be used for photogrammetric purposes, especially close-range photogrammetry as in UAV-based (Linder, 2009).

The basic principle in the field photogrammetry is stereoscopic viewing to be able to gather three-dimensional information from two-dimensional photographs, the principal is that if an object appears on more than two photos, which are taken on different locations, it is possible to calculate the three-dimensional object coordinates (Linder, 2009).

The base of photogrammetry is the transfer of point coordinates, as they are obtained in aerial images, to 3D coordinates which are in an object-space related refence system. This is based on the hypothesis that every point in the image matches to one specific point in the object space. To calculate 3D coordinates the principal point, the origin of the image coordinate system, the focal length, so called camera constant, as the three parameters of the interior orientation must be known. Further the six parameters of the exterior orientation, which are the three position coordinates of the projection center and the angular parameters, this displays the orientation of camera. If all parameters are known it is possible to calculate the image coordinates of an object with known XYZ coordinate, with collinearity equation. To calculate the XYZ coordinates with known image coordinates at least three observations are needed. This means that overlapping images with different viewpoints are required to calculate 3D coordinates from aerial photos (Lemmens, 2011b). To the stereoscopic photogrammetry technique, a new method emerged

since 1990, Structure-for-Motion (SfM), which uses highly redundant iterative bundle adjustments and therefore needs photos which are overlapping to a high proportion. SfM doesn't need information about the camera pose and scene geometry due to the reconstruction of these parameters through automatic identification of matching features in multiple photographs. A significant difference between SfM derived point clouds and traditional photogrammetry is that SfM calculates the camera position and therefore they have no orientation and scale, which results in point clouds that have a relative image-space coordinate system and need to be aligned to object-based real world coordinate systems. This alignment is usually done by either installing ground control points with known coordinates and high visibility before taking the aerial photographs, using well identifiable objects in the resulting point cloud and their counterparts in the real world (Westoby *et al.*, 2012). In this research the SfM technique is used and for the alignment of the point cloud the GPS coordinates of the cameras are used.

The advantage which unmanned aerial vehicle (UAV) based systems have in comparison with airborne or spaceborne systems is the higher spatial and temporal resolution at lower costs. This reason makes UAV-based remote sensing systems really attractive in a variety of scientific fields, as environmental science and forest inventory (Fritz *et al.*, 2013).

The systems used on UAVs are LiDAR systems and cameras for orthophotos, which are used for photogrammetry. UAVs are mostly used for photogrammetry purposes and UAV-based LiDAR systems are rare, because of the high price tag of the LiDAR systems.

1.3. Research Objectives

1.3.1. General research objective

The overall research objective is to compare two remote sensing techniques photogrammetry and LiDAR in order to determine up to which point photogrammetry is an adequate alternative to LiDAR for monitoring savanna ecosystems. This research is focusing on the geographical information technology and is not orientated to ecological factors regarding savanna ecosystems.

To achieve the main objective, this research has two sub-objectives to provide a more detailed comparison. First is the comparison of standard models derived from remote sensing data such

as DTM and CHM, second is the comparison of a tree count in the research area as well as the canopy cover in m², which are key factors in savanna ecosystems.

1.3.2. Research questions

This research aims to answer the overall research question:

For which datasets can photogrammetry be used as a replacement for LiDAR in savanna ecosystems?

Further aims this research to answer more detailed research questions which are aiming to structure the research and give a more detailed comparison:

- Which digital model (DTM, DSM, CHM) can be derived from LiDAR and photogrammetry data?
    - For which digital model is a from photogrammetry data derived model an alternative to the from LiDAR data derived model?
- Which forest parameters can be measured with LiDAR and photogrammetry?
    - For which forest parameters is photogrammetry a useful alternative?

2. Methodology

2.1. Dataset

The Dataset were taken by the RIEGL RiCOPTER with VUX-1UAV, which is an integrated UAV and sensor system. The UAV is an octocopter which can fly up to 30 min and has a maximum payload of 8 kg, so that the system in total weights < 25 kg, so it can be operated under light UAV regulations in most countries.
The VUX-1UAV sensor system is a survey grade laser scanner, which is positioned under the RiCOPTER and has a Field of View of 330° to the flight track. The sensor system operates at a wavelength of 1550 nm and additional to the integrated sensor system two Sony Alpha-6000 cameras were mounted to the UAV.

Figure 4: RIEGL RICOPTER (RIEGL, no date)

This results in an already georectified LiDAR point cloud and in raw photos of the same area, which must be processed.

The photogrammetry datasets were obtained on 12th September 2018, with 2 flights over the study area. For each flight, the two cameras took aerial photos.

Table 1 Number of photos taken during each flight

Flights	Photos taken by camera 1	Photos taken by camera 2
1	374	374
2	489	487

2.2. Software

During this research process different software is going to be used:

- Agisoft Photoscan (now Metashape): for the processing of the photogrammetry data
- LASTools: for the processing of the LiDAR data

- CloudCompare: for the processing of the LiDAR data; alignment of the photogrammetry and LiDAR point clouds; comparison of both methods
- LidR: for processing the point clouds and deriving forest parameters
- ArcGIS Pro: for visualizing

Agisoft Photoscan is an advanced software tool with which it is possible to create professional quality 3D content from images. Based on the newest structure-for-motion algorithms photos can be taken from any angle and objects can be reconstructed, if they are visible in at least two photos. The processing procedure is following 4 main steps to create a DEM (Agisoft, 2018):

1. Camera alignment
2. Generation of a dense point cloud
3. Generation of a surface (Mesh and/or DEM)
4. Texturing of the created surface

CloudCompare is an editing and processing software for 3D point clouds and triangulated mesh. It is designed for direct comparison of dense 3D point clouds and was meant to deal with this huge point clouds on standard laptop.
LAStools is a software package which can be used via a native GUI or it can be added as a toolbox to ArcGIS and other programs. The toolbox contains tools to classify, raster, triangulate, contour, clip, polygonise point clouds, and more.
LidR is a script package for airborne LiDAR data manipulation and visualisation for forestry application. It contains tools for individual tree segmentation, point filtering, classification from geographic data, and more useful tools.

2.3. Data processing workflow

For the processing of the photogrammetry data the processing workflow, which is described in Figure 5, will be used.

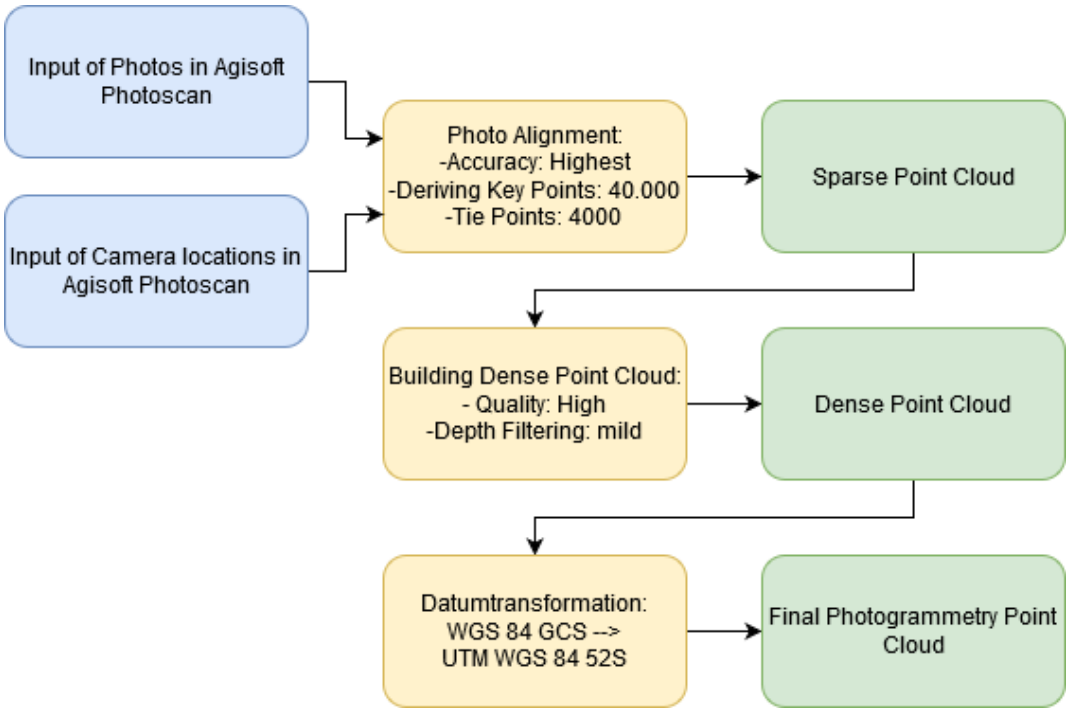

Figure 5 Preprocessing of the photogrammetry data

The LiDAR data is already processed and is available as a georectified point cloud and therefore no data processing is needed.

For data handling reason the point clouds will be cropped to a 100x100 m area in the center of the study area. This area is big enough to answer the research question but is beneficial for data handling.

Next step is to align the two point-clouds so that the comparison delivers accurate results.

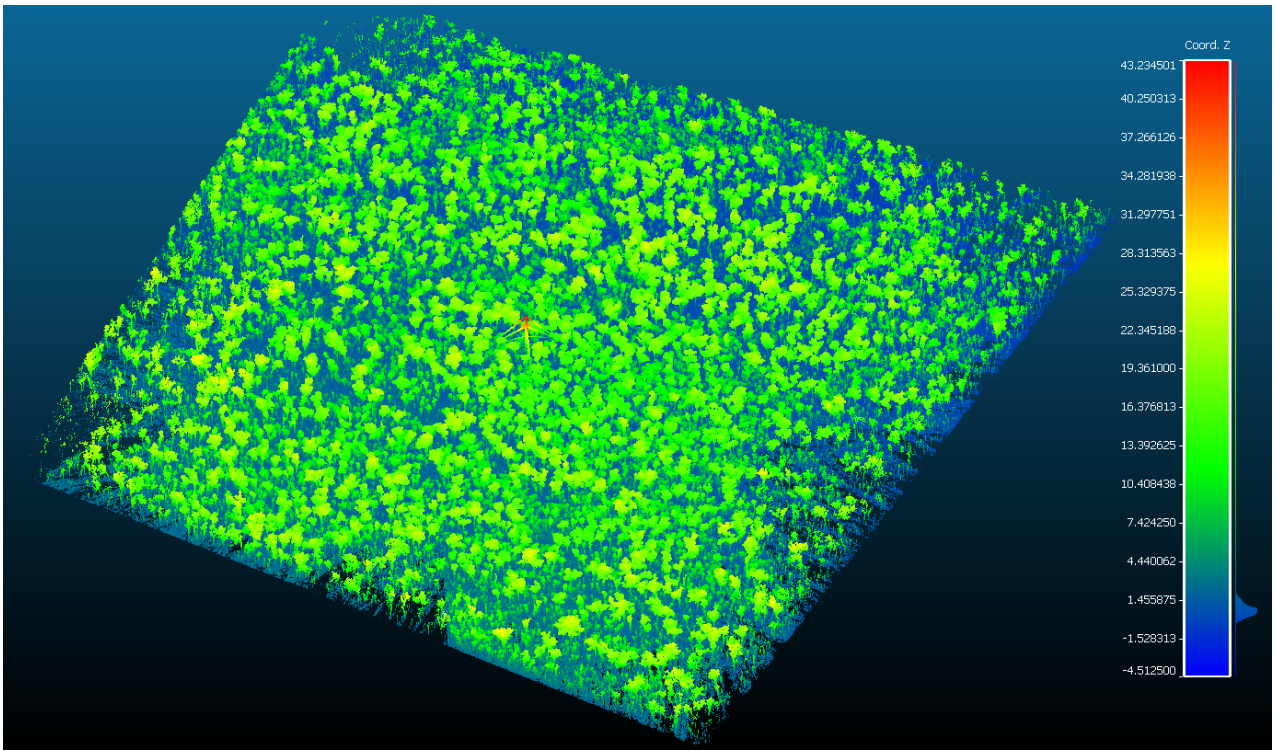

Figure 6 Complete LiDAR point cloud (color scheme: height ramp)

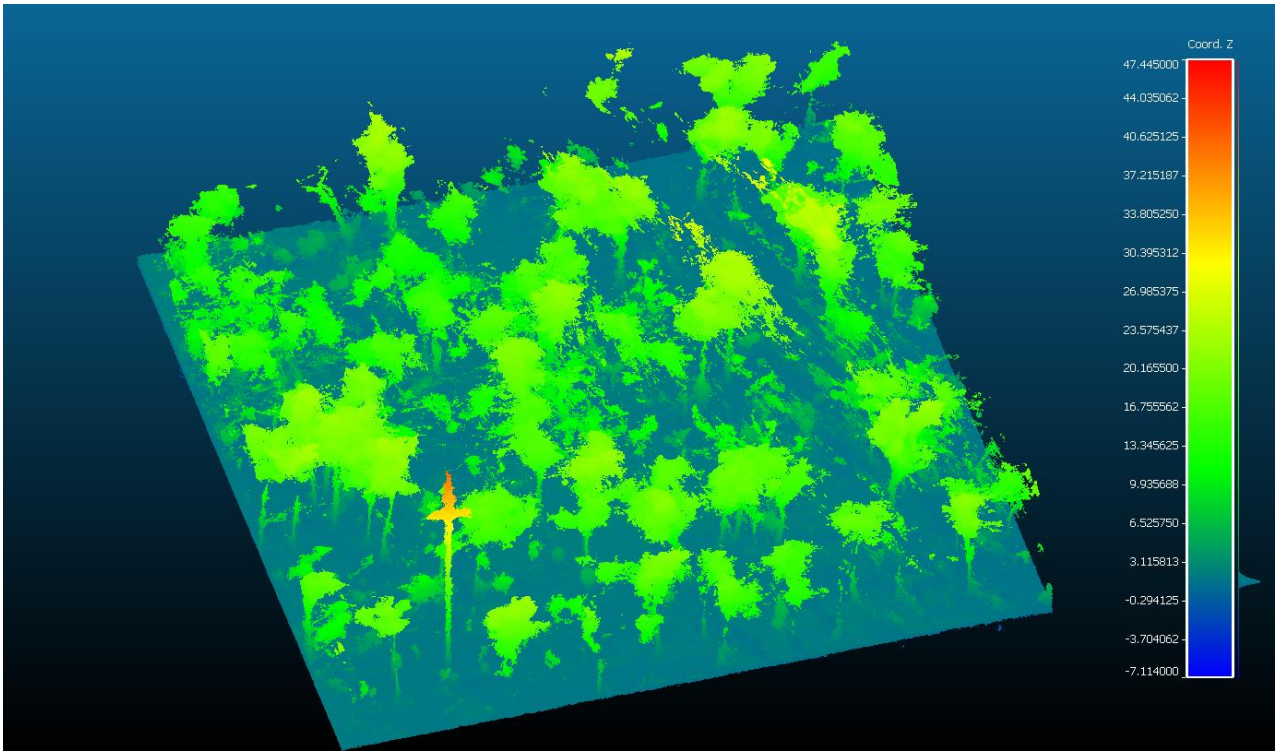

Figure 7 Photogrammetry point cloud (color scheme: height ramp)

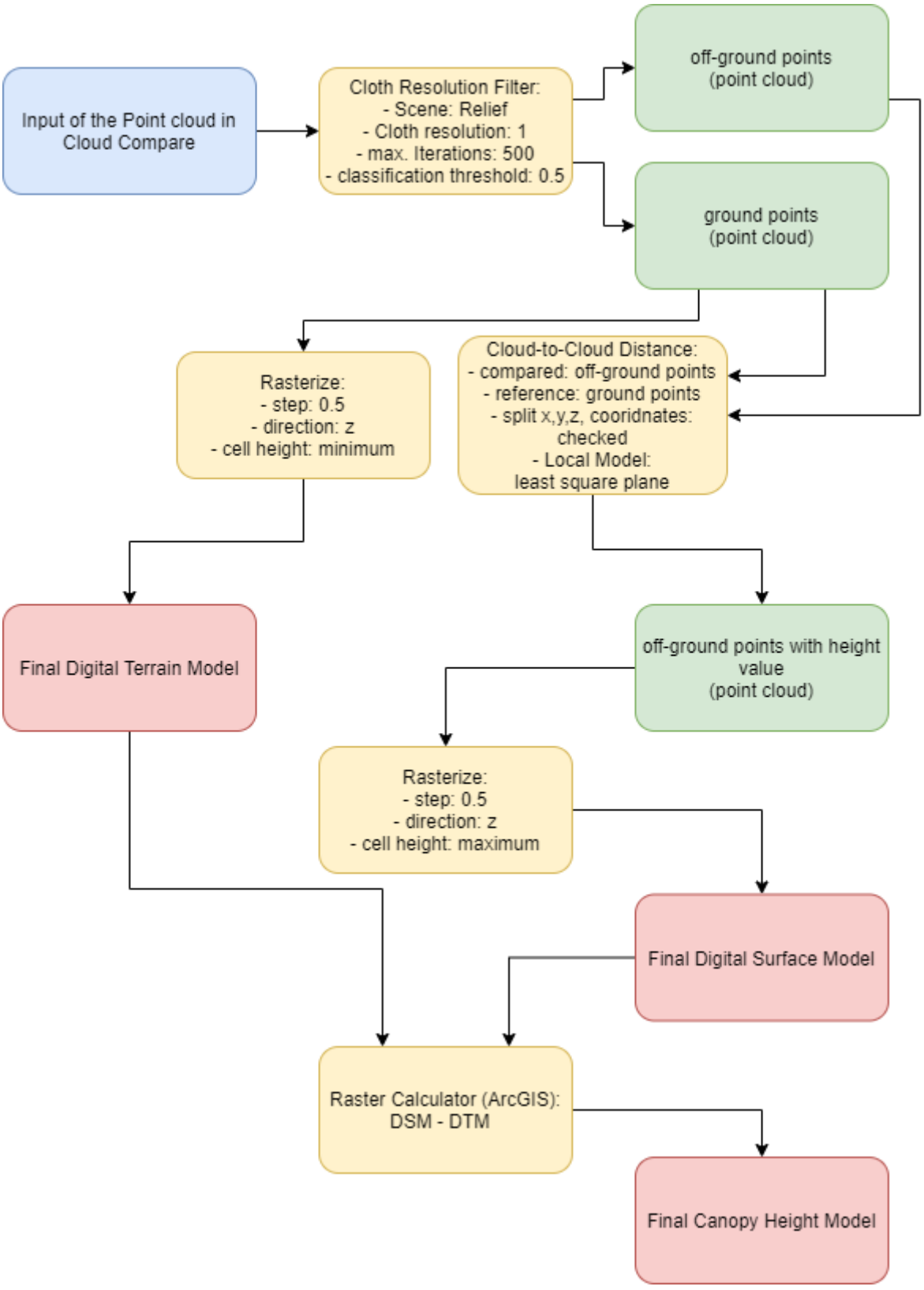

Figure 8 Flowchart diagram of the calculations in CloudCompare

When the point clouds are aligned the construction of the digital terrain model is the next step. Therefore, the lowest point in a raster grid with a resolution of 0.5 m is going to be used to

calculate the DTMs. The resolution of the DTM is set to 0.5 m because this is the highest resolution that can be upheld in the calculations of the further models. Due to the high required computing power it was not possible to ensure a higher spatial resolution for the digital models. Therefore, the models were kept uniform to assure higher comparability. To obtain the best possible outcome the first step is to separate ground points and off-ground points, which is also a vital step for the further calculation of the DSM. The classification in ground and off-ground points is done by using the cloth-simulation filter plugin in CloudCompare. Before the calculation of the final DTM outliers must be removed, especially for the photogrammetry point cloud this is a vital step. Otherwise the calculation approach with the minimum z-values will generate adulterated results, which will affect further results negatively. For the calculation of the DTMs the rasterize tool in CloudCompare will be used, the parameters for the rasterize tool can be found in figure 8. When both DTMs are constructed a difference map will be calculated with the Raster Calculator in ArcGIS Pro to evaluate the differences between the two DTMs. Also, statistics as mean, median, minimum, maximum difference of the difference maps as well as from the both DTMs is going to be used to evaluate the differences between the DTMs.

Further a digital surface model will be constructed, by using the cloud-cloud distance tool in CloudCompare. This tool needs as input the ground points and off-ground points as they were created with the CSF plugin in the creation process of the DTMs. For computational reason the parameter ‘Local Model’ is set to ‘Least Square Plane’, because otherwise the computers used in this research couldn’t finish the calculations. For the comparison of photogrammetry and LiDAR a difference map is going to derived from the two created DSMs, here the same method in ArcGIS is used as in the DTM calculation. Further statistics of the difference maps as well as the statistics from the two created DSMs is going to be used for the evaluation.

The last models which will be derived from the two point-clouds is going to be a canopy height model. The CHMs will be constructed by using the Raster Calculator in Esri’s ArcGIS. For both the LiDAR and photogrammetry derived models the same technique is going to be used, to make sure that the results can be compared in chapter 4. The CHM will be calculated by subtracting the DTM from the DSM. The next step is to derive a difference map of both canopy height models to evaluate the differences. The difference maps are calculated again by using the raster calculator in ArcGIS. For this task also statistics of the difference map and the both CHMs are going to be used.

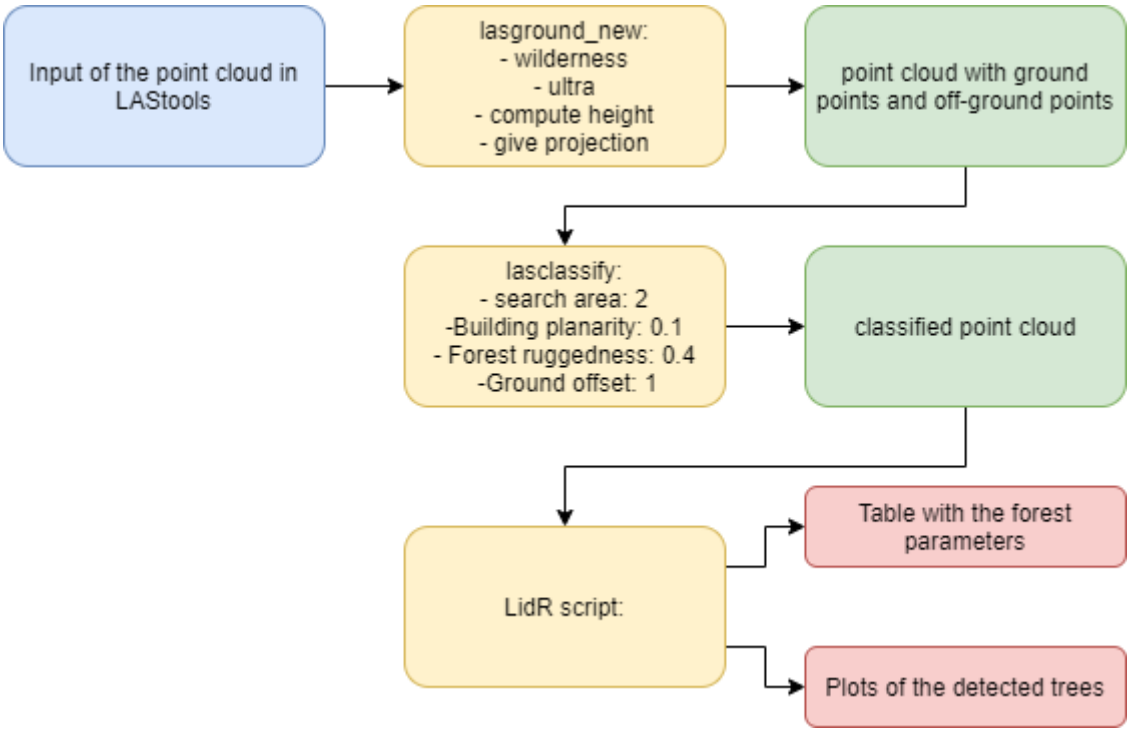

Figure 9 Flowchart diagram of the forest parameter calculation

The forest parameters which are going to be compared are, number of trees, crown size, average tree height, and m^2 of the gaps.

To calculate these parameters, first the point clouds are classified by using the LAStools lasground_new and lasclassify applications. These steps are needed because the lastrees function in the LidR library, needs a classified point cloud as input dataset. The next steps in the R script is to calculate a DTM again, which is then used to get a point cloud with normalized height values the lasnormalize function is used. With a filter the vegetation points of the respective point cloud are selected and then the lastrees function is used to calculate the single trees of the input datasets. For the tree segmentation the li2012 algorithm is used, compared to the other available dalponte2016, silva2016, and watershed algorithms, which can be used, li2012 doesn't require an CHM as further input to the LAS dataset. The li2012 algorithm requires three further input parameters, R is the search radius with the default value of 2, Speedup is the maximum crown size with the default value of 10, and hmin is the minimum height of a detected tree with the default value of 2. These were set to R = 5, Speedup = 7.5, and hmin = 5. These parameters where chosen by trying different parameter setting for a small test area. This can result in distorted trees, because cut of branches are getting allocated to smaller trees or bushes. A distortion can also occur when the radius is set too high, because then smaller trees get mistakenly allocated to higher trees, and lead to the small number of detected

trees. The chosen parameter set results focuses on displaying the higher trees as best as possible while not allocating all smaller trees to higher trees in their surroundings.

Afterwards important parameters as height, mean x and y coordinate, point count for the tree, and principal component analysis (PCA) score, are being calculated during a for-loop over every detected tree and saved as a table. The PCA score means that the relation between the main axes is used to check if the detected trees are proper trees. If the ratio is higher than 1.2 it is assumed that it is not a proper tree and the value 0 is assigned to the tree. If the ratio is lower than 1.2, it is assumed that it is a real tree and the PCA value of 1 is assigned to the tree.

Further the diameter at breast height (DBH) is calculated using an R script. For the DBH again a for-loop is used, where for every tree the points in a height between 1.3 and 1.5 m are extracted. If the resulting variable is not empty, the result is plotted. In the next script trees with similar coordinates are searched and the distance between the mean coordinates is calculated. This is achieved by a for loop over all trees in the photogrammetry dataset, then a for-loop over all trees in the LiDAR dataset. In the second loop the script checks for similar coordinates with if-else statements, which are checking if the mean coordinates of the trees in the LiDAR datasets are in a range of +/- 3m of the mean coordinates of the trees in the photogrammetry dataset.

For all comparisons, the LiDAR data will be the reference, to which the photogrammetry derived data will be measured.

3. Results & discussion

In this section the LiDAR point cloud and the photogrammetry derived point cloud are going to be analyzed. For this statistics, as for example point density and total points, are going to be used to check for differences in the input datasets.

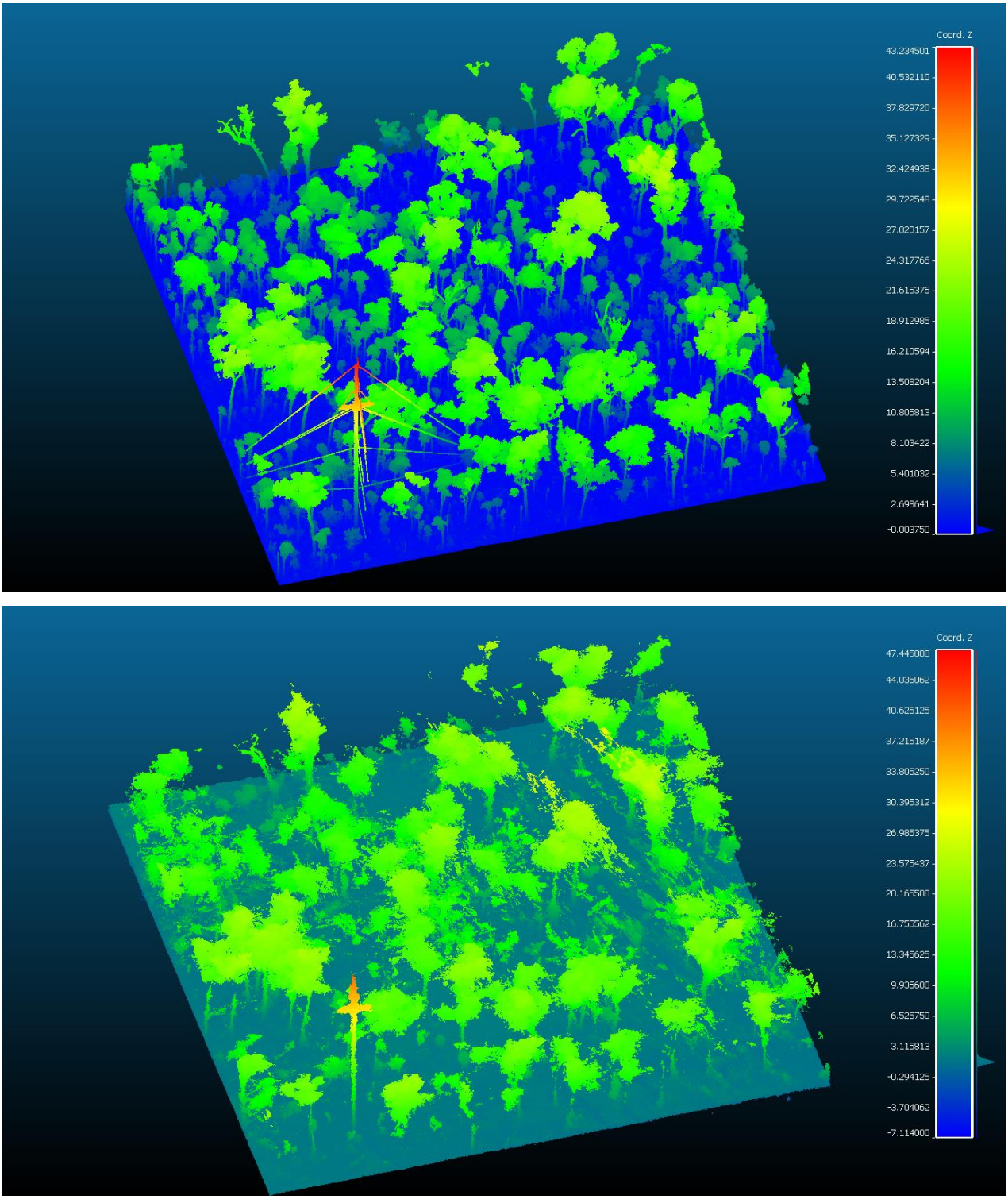

Figure 10 Input point clouds for the Model calculations (top: LiDAR, bottom: photogrammetry, color scheme: height ramp)

Both point clouds are clipped to an extent of 100x100 m, the complete input LiDAR point cloud has an extent of 800x800 m whereas the calculated point cloud from photogrammetry has an extent of 300x300 m. This because that the SfM techniques used to construct the point cloud from photos, needs high computational power. Furthermore, SfM requires overlapping photos this has the consequence that only areas within the flightpaths can be used as research areas. LiDAR on the contrary measures also outside the flightpaths and can therefore display bigger areas. The specifications of the computers available at Utrecht University limited the research area to the aforementioned 100x100 m. Therefore, the point cloud calculated had an extent of 300x300 m and was then cropped to the extent used for the further calculations.
Some key figures of the point clouds used as input for the generation of the digital models can be seen in Table 2.

Table 2 Key figures of the 100x100 m input point clouds

Input point clouds	LiDAR	Photogrammetry
Total points	29.733.861	52.118.141
Point density per m^2	2.962,72	4.890,97
Ground point density per m^2	1825,78	2.656,92
Off ground point density per m^2	1.256,83	2.357,55

As it can be seen in the table the two point clouds largely differ from each other and the LiDAR point cloud has in total less points than the photogrammetry. The difference of the point distribution between ground and off ground points is not big, for the LiDAR point cloud 62% are classified as ground points and 38% as off-ground points, and for the Photogrammetry dataset it is 54% ground and 46% off-ground points.

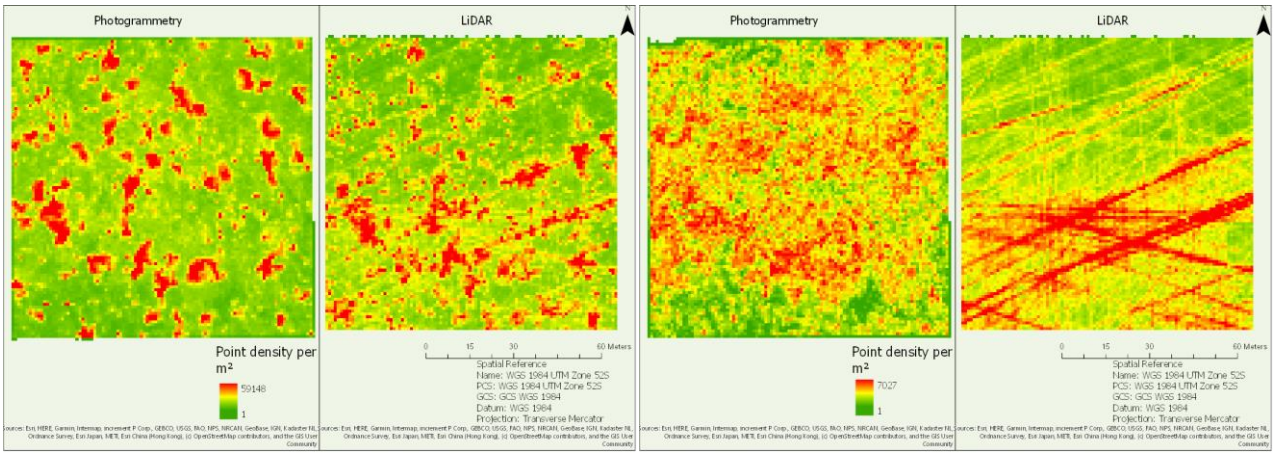

Figure 11 Spatial distribution of point density per m² (left: total points, right: ground points)

The point density of the photogrammetry point cloud is overall higher than of the LiDAR point cloud. The point density of the photogrammetry point cloud is highest where dominant trees are located. Due to the photogrammetric method of the point cloud calculation this distribution is to be expected, because higher points are better identifiable in photos and can therefore be better reconstructed. In the photogrammetry point cloud, the highest points have the highest point density and show therefore a more vertical pattern. The spatial distribution of the point density of the LiDAR point cloud shows more a horizontal pattern. That means that the point density is higher in area closer to the flight path, where the laser beam has the fewest obstacles. The spatial distribution of the point density of the LiDAR ground points shows a spatial pattern more clearly, whereas in the photogrammetry dataset no clear pattern can be found.

3.1. Digital Terrain Model

The DTM constructed from LiDAR and photogrammetry can be seen in Figure 12, and it can be observed that the LiDAR DTM is smoother than the photogrammetry derived DTM. This can be seen throughout the photogrammetry DTM map. The LiDAR DTM shows an even gradient from the higher southwest corner to the lower northeast corner. Due to the higher accuracy of the LiDAR dataset, it is possible to detect the road in the DTM. The photogrammetry DTM on the contrary is rougher in the comparison. An explanation for this is, that the understory vegetation in the savanna woodland creates the uncertainty. The less vegetation is near the ground and the clearer the photo of the ground is the higher detailed the photogrammetry DTM gets. Another explanation for the noisier photogrammetry DTM can be the mild depth filter parameter which was chosen during calculating the photogrammetry point

cloud. Therefore, an option to receive a more detailed DTM with SfM is to set the depth filtering parameter more aggressive in the point cloud creation process.

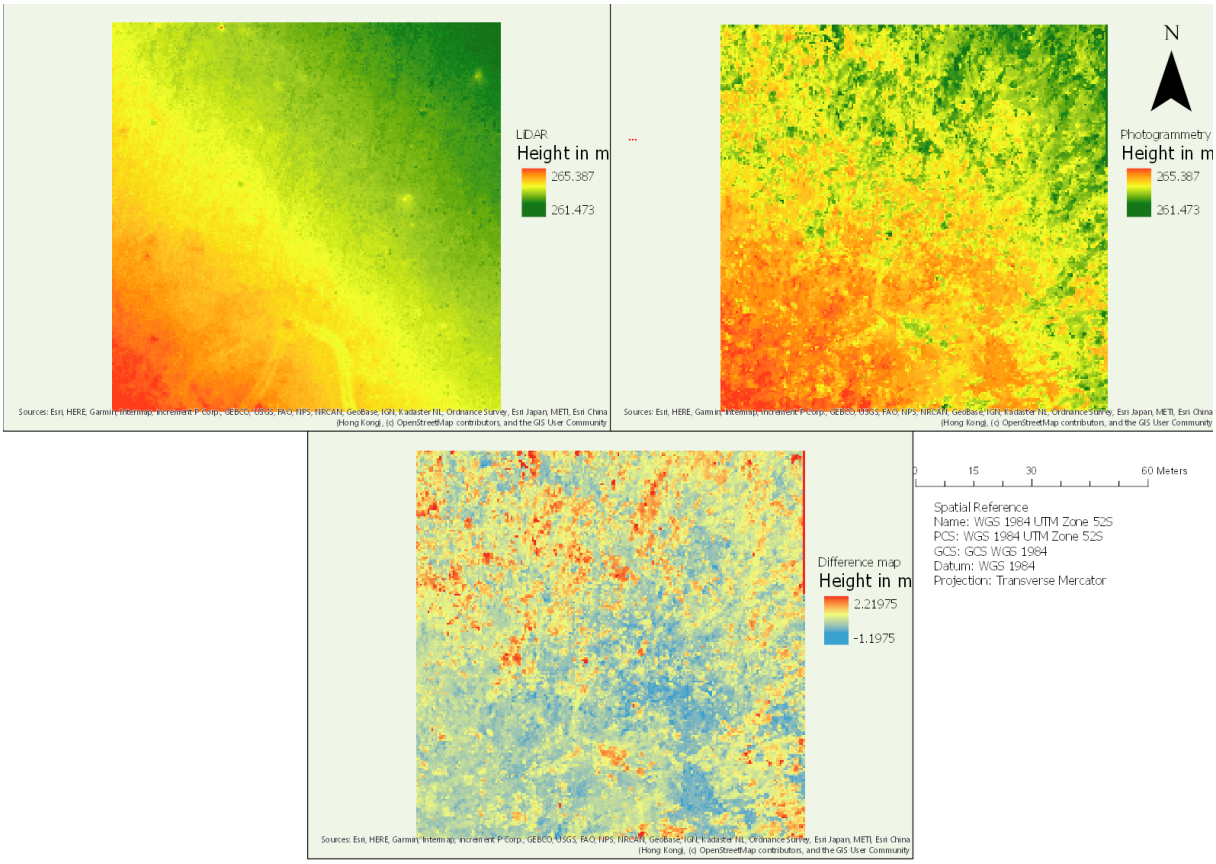

Figure 12 DTMs derived from LiDAR and photogrammetry, and the difference map

In general, it can be stated that the photogrammetry DTM is close to the LiDAR DTM, the maximum is 1 m higher and the minimum 2 m lower than the LiDAR reference DTM and the mean difference is -0.7 m, shown in Table 3.

Table 3 Basic statistics of the Digital Terrain Models

DTM elevation in m	LiDAR	Photogrammetry	Difference Map
Mean	263.88	264.57	-0.69
Median	263.87	264.59	-0.71
Min	263.52	261.47	-1.20
Max	264.39	265.39	2.22

The histograms of the digital terrain models are shown in the Figure 13, Figure 14, and Figure 15.

The histogram of the photogrammetry DTM show the outliers at the minimum end of the range. The LiDAR histogram on the other hand shows a more equal distribution. The histogram of the difference map underlines the differences between the LiDAR and the photogrammetry DTM. The difference map histogram shows that most of the photogrammetry values are lower than the reference values in the LiDAR dataset, with a centration around the mean value of the difference map at -0.71m, as can be seen in Figure 15.

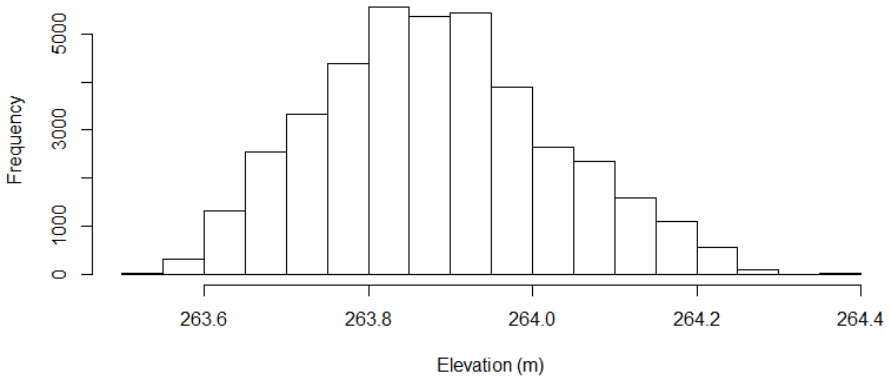

Figure 13 Histogram of the LiDAR DTM

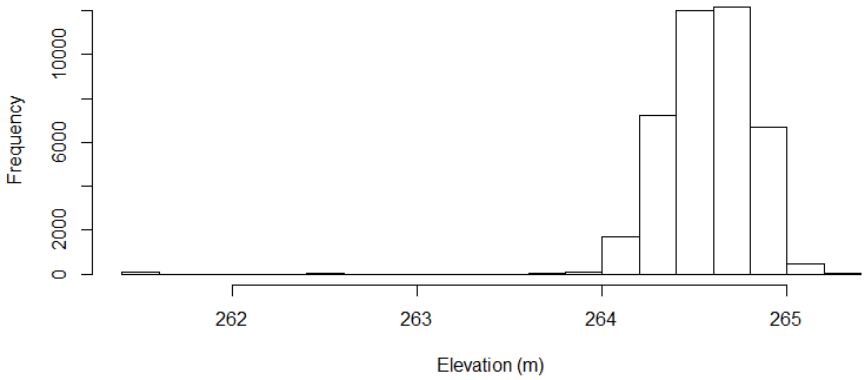

Figure 14 Histogram of the photogrammetry DTM

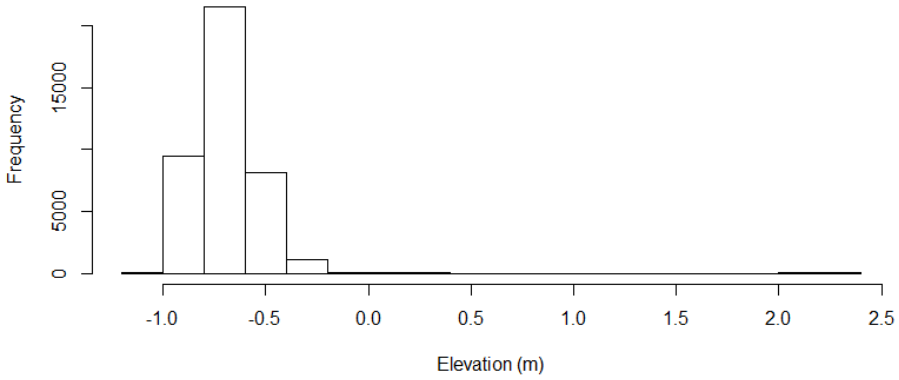

Figure 15 Histogram of the DTM difference map

In the overall comparison of the two digital terrain models it can be stated that the absolute height values from the photogrammetry derived model are 0.7 m lower than values from the LiDAR derived model. This can be a result of the photogrammetric calculation of the point cloud and the high above ground vegetation density, which leads to a bigger inaccuracy regarding the ground points. For the LiDAR point cloud on the other hand, the bare ground back scatters the LiDAR impulse directly and therefore results a clear ground point cloud. Another explanation can be that the coregistration is not perfect, which can be explained by the difficulty of finding corresponding points in both datasets. Coregistration is the process of spatial alignment of two datasets, so that corresponding points have the same coordinates (Goshtasby, 2012). The savanna ecosystems make it extremely hard to find distinctive points in both datasets which are suitable. If the DTM has a high enough accuracy depends on the use case and application, but it can be stated that it is possible to derive a DTM from the LiDAR and photogrammetry point cloud.

3.2. Digital Surface Model

For the DSM the differences in data quality between the LiDAR and photogrammetry point clouds gets more obvious than in the comparison of the DTMs, as seen in the maps in Figure 16. The higher capability to gage small objects can be noticed, by comparing the tower in the southwest corners of the maps. In the LiDAR map the tensioning cables of the tower can be identified, whereas in the photogrammetry map only the center pole can be identified. Further it can be identified in the difference map, because around the tree crowns the highest minimum and maximum values can be noticed.

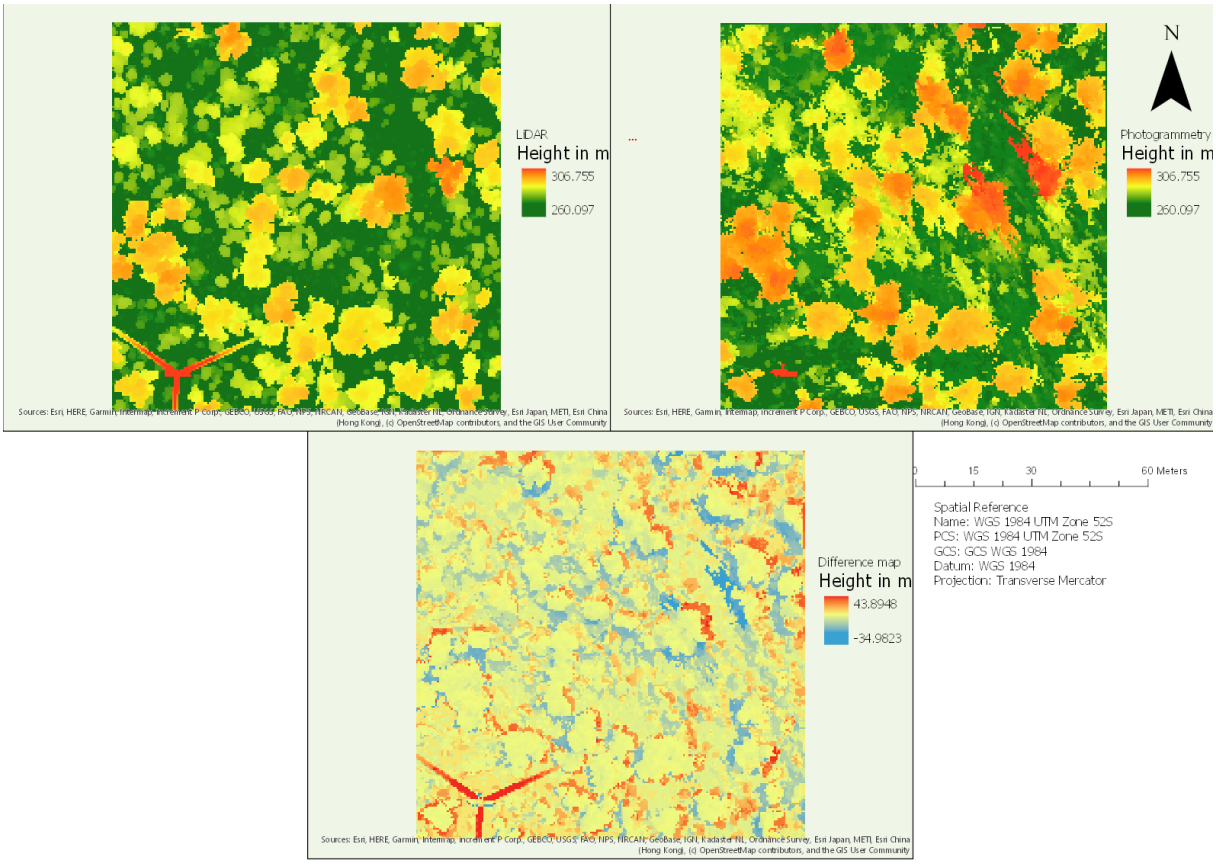

Figure 16 DSMs derived from LiDAR and photogrammetry, and the difference map

The biggest difference can be observed in the northeast corner, the tree crowns there are bigger in the photogrammetry dataset, what entails that there are higher differences in the difference map.

The difference map also shows a clear difference in the representation of trees between the two datasets, this can be observed in the center of the maps. In the LiDAR map, single trees of different height can easier be identified than in the center of the photogrammetry map, here the tree crowns merge into each other and make it more difficult to distinguish between the different trees.

The basic statistics of the photogrammetry map are close to the reference values of the LiDAR map, with a difference in the mean value of 0.56 m, further are the minimum and maximum value approximately 3 m lower than the reference LiDAR values.

The extreme minimum and maximum values for the difference map can be explained through the calculation method, because for the photogrammetry map is subtracted from the LiDAR map with the ArcGIS Rastercalculator. This results in the circumstance that, if a raster cell in the photogrammetry map has a higher value than the reference cell in the LiDAR map, the result

has a negative value. The negative values in the difference map indicate that these cells have higher height values in the photogrammetry map than in the LiDAR map. This can be caused by differences in the tree crown representation.

Table 4 Basic statistics of the Digital Surface Models

DSM elevation in m	LiDAR	Photogrammetry	Difference Map
Mean	271.64	272.20	-0.56
Median	270.50	272.01	-0.58
Min	263.70	260.10	-34.98
Max	306.75	303.47	43.89

The distribution of the values can be seen in the Figure 17, Figure 18, and Figure 19, which are the histograms of the digital surface models. The basic distribution of the two histograms is similar, the biggest part of the values is distributed towards the lower end of the occurring values.

Interesting is that the photogrammetry histogram shows a bar for values at 260 m followed by a gap and then the next bar is at approximately 265 m. The first bar and the gap mark the biggest difference between the photogrammetry and the LiDAR histogram and could be explained with the mild depth filter. The mild depth filter creates more outliers compared to more aggressive options, which can lead at a spatial resolution of 0.5 m to raster cells with values of the outliers. This also benefits from the chosen methodology, because before creating the DSM a cloth-simulation filter is used to classify and separate ground and off-ground points and the more aggressive the depth filter is the better can cloth-simulation filter distinguish between ground and off-ground points.

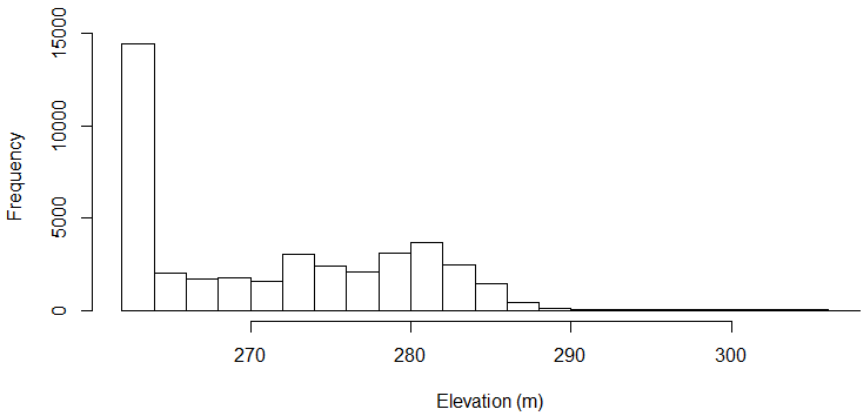

Figure 17 Histogram of the LiDAR DSM

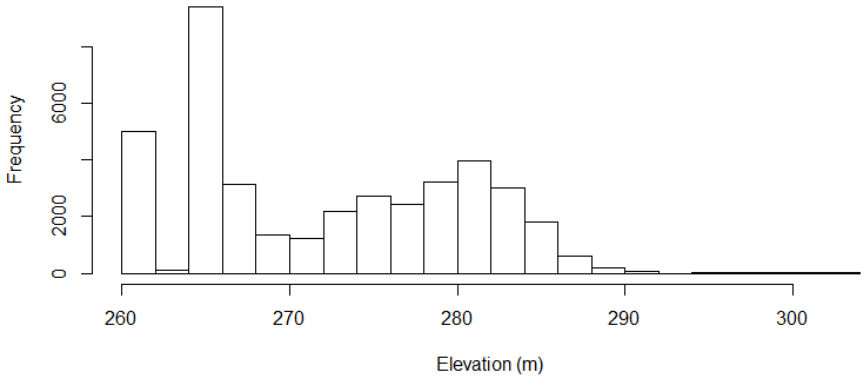

Figure 18 Histogram of the photogrammetry DSM

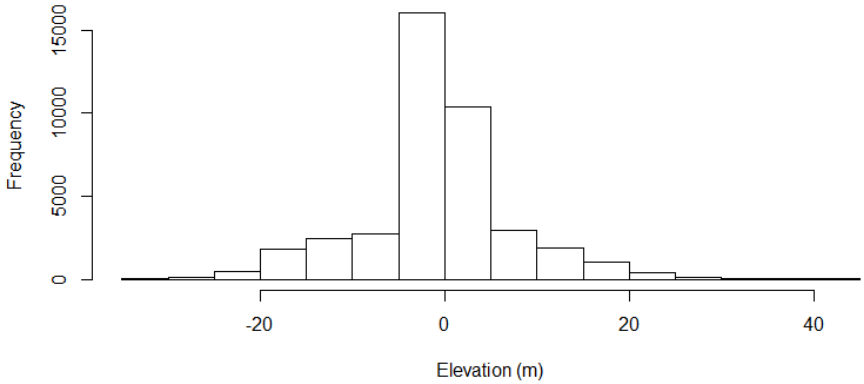

Figure 19 Histogram of the DSM difference map

For the histogram of the difference map the distribution concentrates around 0 m and seems normal distributed.

3.3. Canopy Height Model

The last digital models which were calculated in this research are two canopy height models and the respective difference map, as can be seen in Figure 20. As in chapter 2.3. described they were calculated by the subtraction of the DTM from the DSM. Due to the calculation method the two CHM models are similar to the DSMs and also the respective difference map. The biggest differences between the two models are therefore area around the tower and the areas

directly around the tree crowns, where the difference in the reconstruction of the trees is the biggest between the LiDAR dataset and the photogrammetry dataset.

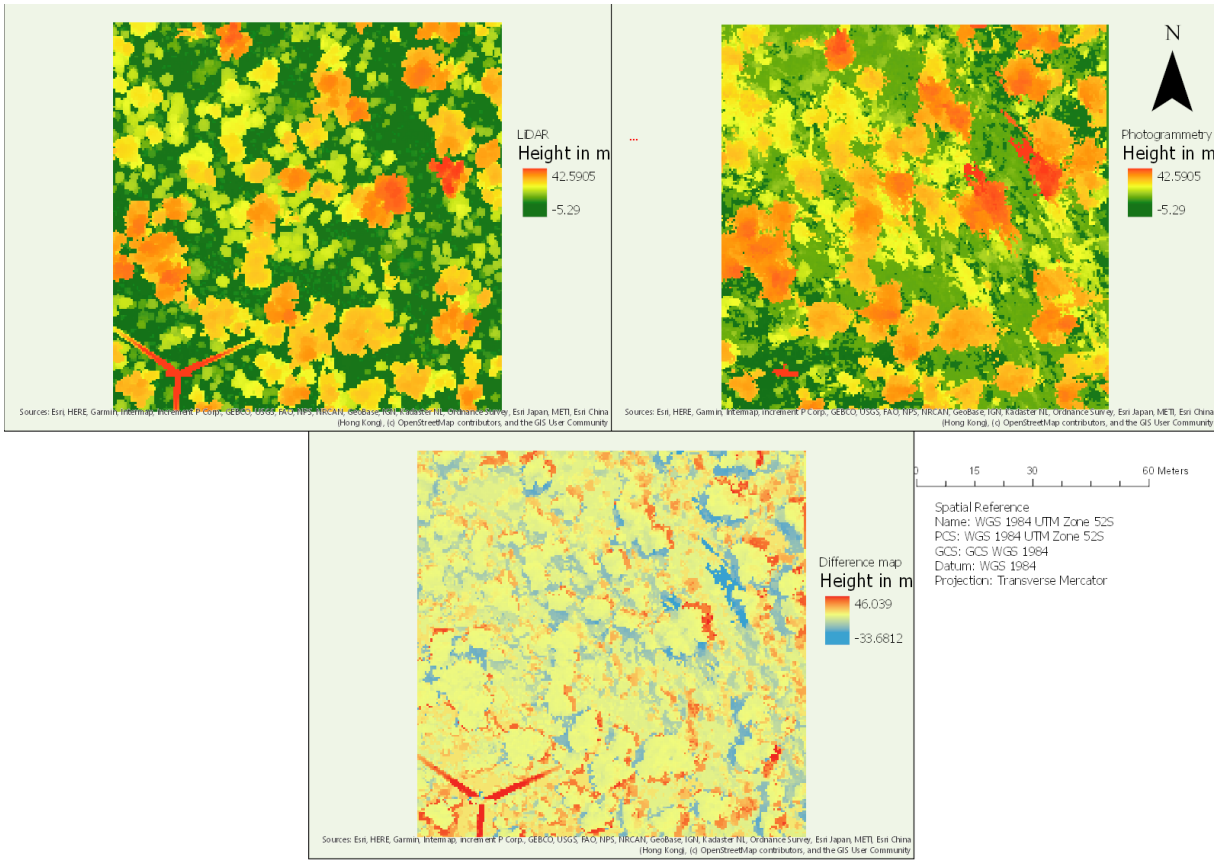

Figure 20 CHMs derived from LiDAR and photogrammetry, and the difference map

The close results of the two remote sensing methods can also be observed, when considering the mean value of the difference map, which is 0.12 m. Interesting is here that the mean value for the LiDAR dataset is 7.75 m and for photogrammetry it is 7.64 m. Big differences occur for the minimum and maximum differences, the minimum value of the LiDAR dataset is -0.69 m, compared to the minimum of -5.29 m of the photogrammetry dataset. This is interesting because the DSM is subtracted by the DTM and therefore the lowest values are expected to be around 0 m as seen with the LiDAR dataset. The difference between the maximum and minimum values of the photogrammetry DSM are approximately 3 m lower then then LiDAR values, for the CHM the difference is with approximately 4.3 m higher. In contrary to the bigger difference for the extreme values the for the mean value the opposite is the case, is the difference for the DSM -0.56 m is it for the CHM only 0.12 m. An explanation for this is that the uncertainty in the photogrammetry dataset gets bigger towards the ground and by the subtraction of the DTM from the DSM these uncertainties getting reduced. The expected minimum values for the CHM

were expected to be close to 0 m and further that the values are positive. This is caused by the methodology, because an algorithm is used to classify the points in ground and off ground points, this can lead to points mistakenly allocated to the false group and in the next step in the rasterization these outliers can lead to a distortion and result in the negative minimum values for the CHM.

Table 5 Basic statistics of the Canopy Height Models

CHM elevation in m	LiDAR	Photogrammetry	Difference Map
Mean	7.75	7.64	0.12
Median	6.68	7.45	0.08
Min	-0.69	-5.29	-33.68
Max	42.59	38.55	46.04

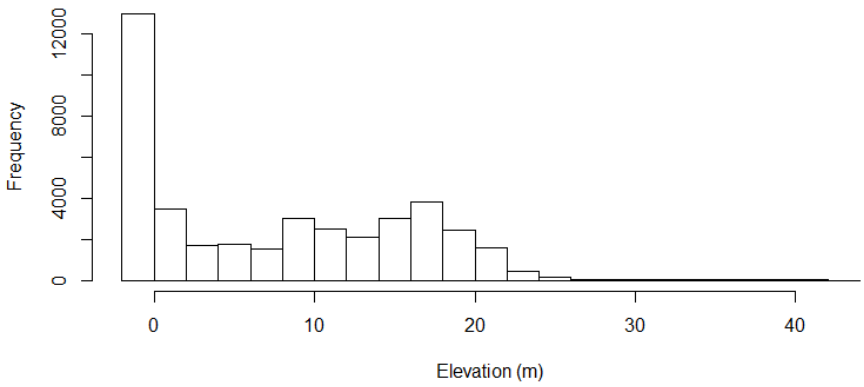

Figure 21 Histogram of the LiDAR CHM

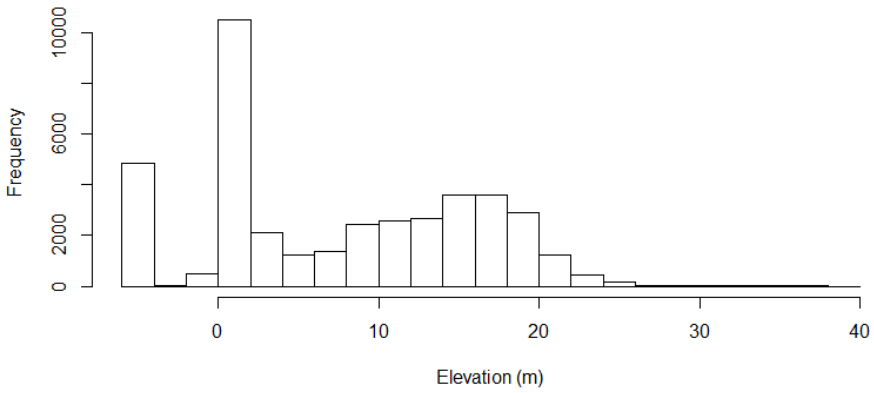

Figure 22 Histogram of the photogrammetry CHM

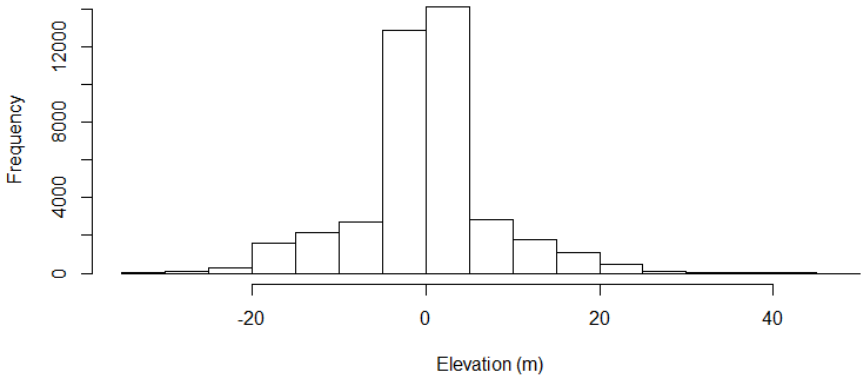

Figure 23 Histogram of the CHM difference map

The histograms of the CHMs chow a similar distribution as the histograms of the DSMs as well as the maps in Figure 20 show similar patterns as the maps for the DSMs. The similarity between the histograms of the LiDAR derived DSM and CHM is the same for the photogrammetry dataset. For both datasets the distribution in the histograms is for both models similar. The histogram for the difference map is slightly different for the CHM compared to the DSM difference map histogram, with the slight shift from the maximum distribution from below to above 0 m.

3.4. Forest Parameters

In Figure 24 the output of the tree detection algorithm can be seen, and it can be observed that the tree count in the LiDAR dataset (on the left) is similar to the photogrammetry dataset (on the right). It can further be stated that the classification algorithm of the lastools suite was not able to rightfully classify the tower, because it is still in visible in Figure 24.

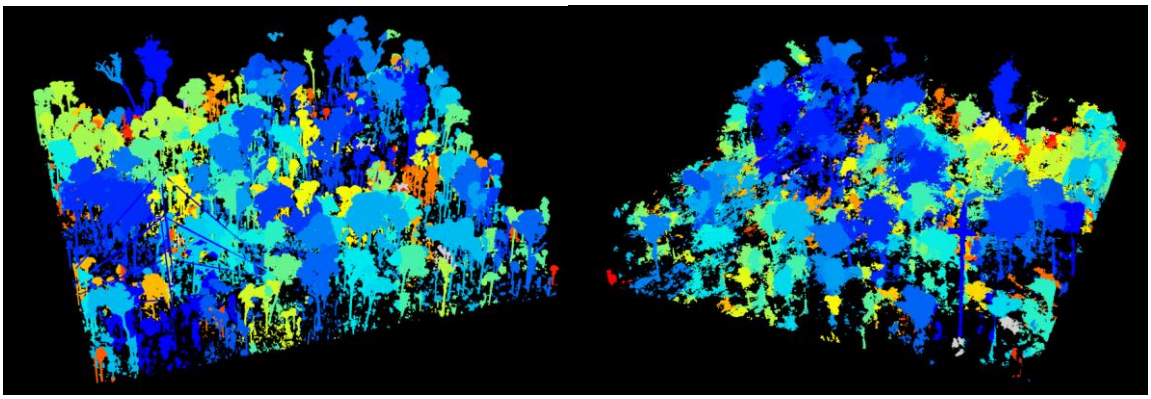

Figure 24 Output of the tree detection algorithm (left: LiDAR, and right: photogrammetry, color scheme: treeID)

The key figures from the result of the tree segmentation show comparable results between the LiDAR and photogrammetry point clouds. So is the canopy coverage in the LiDAR data 80% compared to 82% in the photogrammetry, with the respective 20% gap area in LiDAR and 18% in the photogrammetry data. All further key figures as mean height, mean crown area, and mean PCA ratio show just slight differences between the two datasets.

It must be stated that the PCA ratio and the number of trees with a PCA score of 1, are just indicators if the trees shape is regular or not. Further, due to the segmentation method of the algorithm, which cuts of every point outside the radius, even if the points represent a branch which is part of the tree in reality. Also is the height composition of the savanna woodland vegetation a challenge for the algorithm, because the range of tree height is from ~5 – 25 m, and the algorithm starts from the highest point. This leads to the circumstance that if parts of lower trees reach into the radius of a higher tree the parts getting allocated to the higher tree and doesn't get allocated to the actual tree it belongs to. This leads to tree crowns as it can be seen in Figure 25 in the top view for the LiDAR tree number 91.

Table 6 Forest Parameters

Forest parameter	LiDAR	Photogrammetry
Tree count	189	209
Canopy area total (in m^2)	7972.4	8664.5
Gap area total (in m^2)	2027.6	1957.4
Count of trees with a PCA score of 1	14	20
Mean height of the trees (m)	15.1	16.2
Mean crown area (m^2)	42.2	41.5
Mean PCA ratio	2.1	2.4

In order to determine the best parameter setting for this research different parameter settings were tested in an 20x20 m test area. For the three parameters the steps 2, 5, 7.5 and 10 were tested in all variations to each other. The number of detected trees differed from 6 (R=10, SpeedUp=10,hmin = 5) to 22 (R=2, SpeedUp=5, hmin=5) for the LiDAR and from 4 (R=10, SpeedUp=10,hmin = 5) to 24 (R=2, SpeedUp=5, hmin=5) detected trees for the photogrammetry dataset. The biggest influence has the maximum crown size parameter, because is it set to small radius every point outside that radius is getting cut of and are no longer

allocated to the right stem. Some results for the LiDAR test area can be seen in Table 7, which shows the influence of the different parameter settings on the results on the tree count.

Table 7 Tree count for different parameter settings for a LiDAR subset

Search radius = R	Maximal crown size = SpeedUp	Tree count
10	10	6
5	10	13
10	5	17
5	5	18

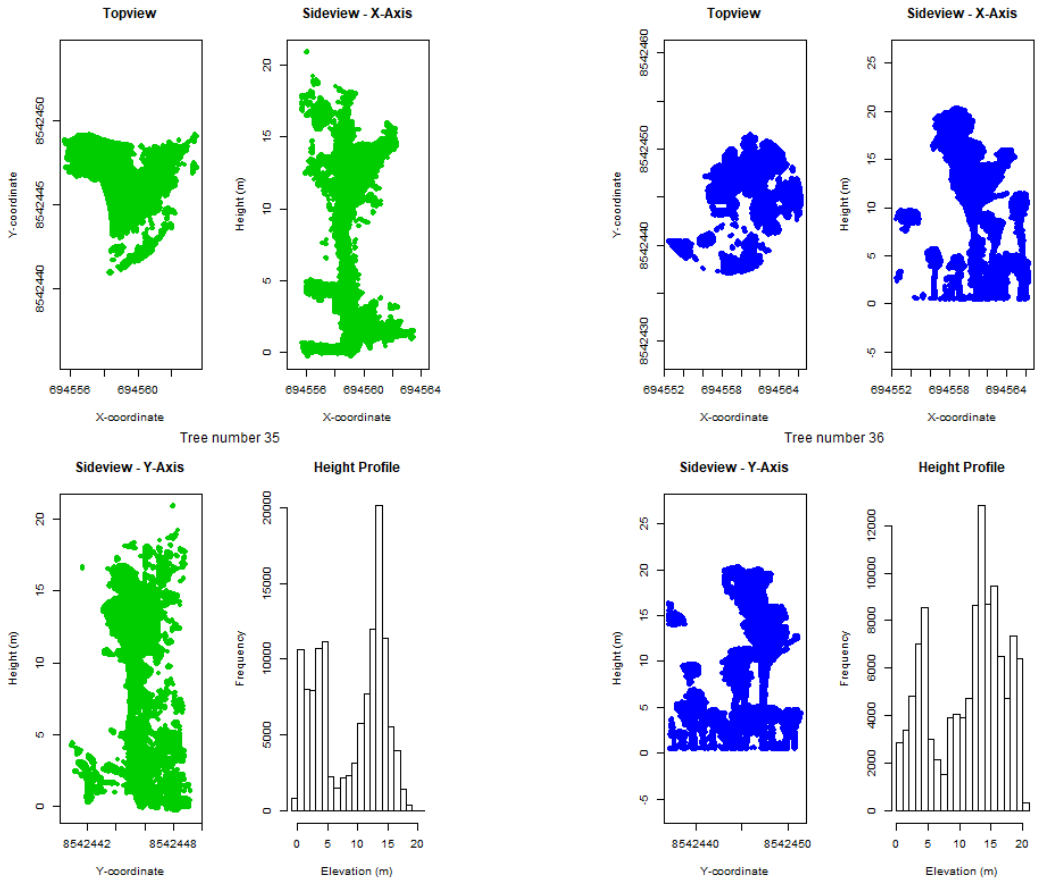

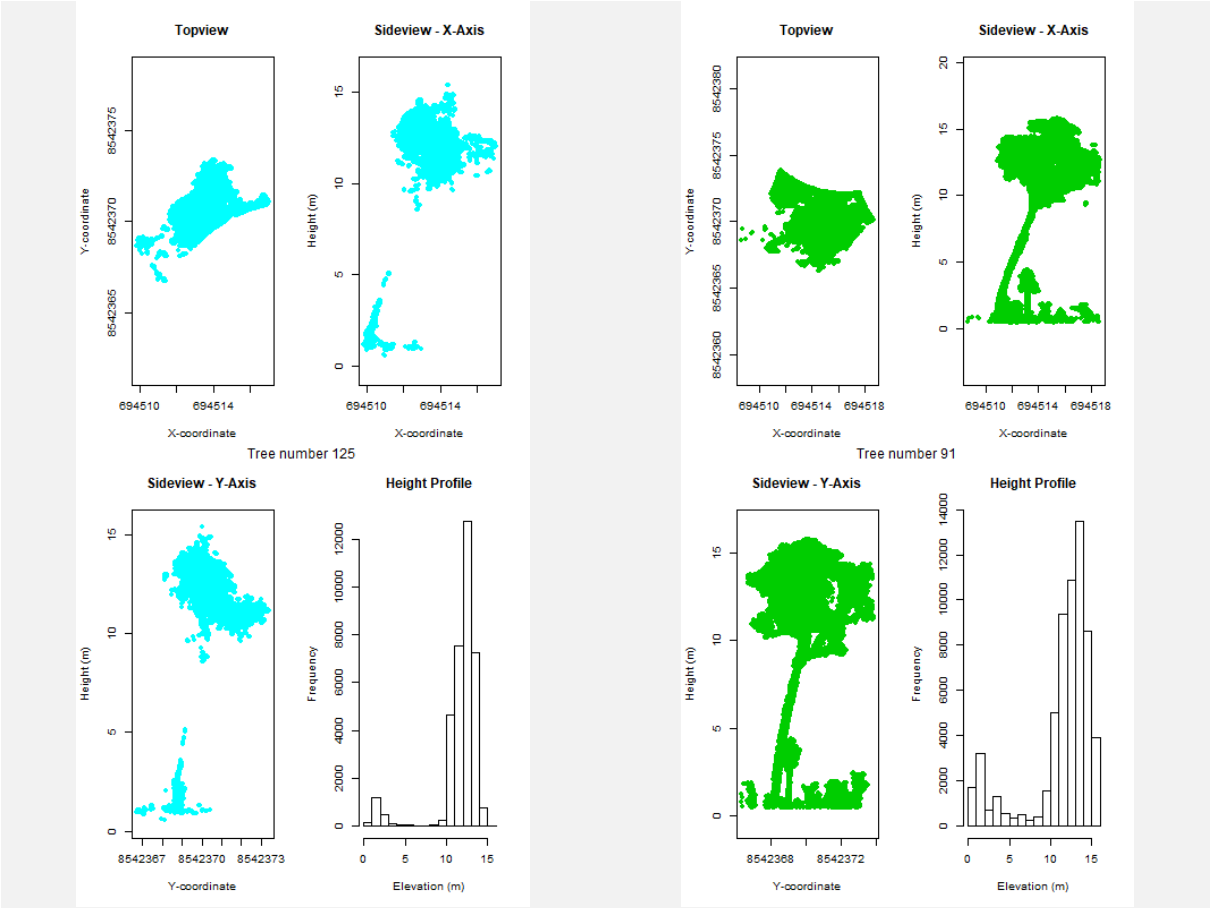

Figure 25 Single results of the detection algorithm (Photogrammetry on the left and LiDAR on the right)

Figure 25 shows two trees, on the left in the photogrammetry dataset and on the right in the LiDAR dataset. According to their mean coordinates tree number 35 (photogrammetry) and tree number 36 (LiDAR) are the same tree and tree number 125 (photogrammetry) is the same as tree number 91 (LiDAR). The tree numbers refer to the overall segmented trees and the treeid which the trees get assigned when running the lasstrees function.

The result sheets for Tree nr. 35 (photogrammetry) and 36 (LiDAR) show a show a significant difference in the vertical distribution of the points. Whereas for LiDAR the vertical point distribution is constant, which doesn't mean that for all detected trees there are the same percentage of points near the ground and at the tree crown is the same, but that LiDAR is able to penetrate the vegetation cover and therefore is able to get high quality results independent of the flight path or sun position. For photogrammetry on the other hand the line of sight is determining the resulting quality. Is a tree stem not visible in the pictures because of high understory vegetations cover or because of the flight angle the tree crown hides it, at least parts of the stem can't be constructed by SfM.

The DBH could not be calculated in either of the both datasets. In the LiDAR dataset the lastree function of LidR grouped shrubs and little trees together under the same treeid, which makes it

in the following not possible to estimate the DBH. In the photogrammetry dataset it was also not possible to estimate the DBH for any tree, this can be caused by the problems of SfM to reconstruct the stems properly, because understory vegetation prevents the detection of the main stem. Also, the same problem as for the LiDAR dataset occurred and understory vegetation got assigned to a main stem and gets the same treeid. Figure 26 shows two examples of the DBH points for the same tree, one from the photogrammetry dataset and one from the LiDAR dataset, where the problems can be seen which prevent an automated approach for the DBH estimation. The main problem for the LiDAR dataset was that it was not possible to detect one single stem for the DBH estimation. In the photogrammetry dataset on the other side the main problem was the lack of points at the right height. In neither of the two datasets was a single tree where the DBH could be estimated, in a scripted way. Presumably, the only chance to estimate the DBH is to crop out single trees in the datasets, remove the outliers and then calculate the DBH.

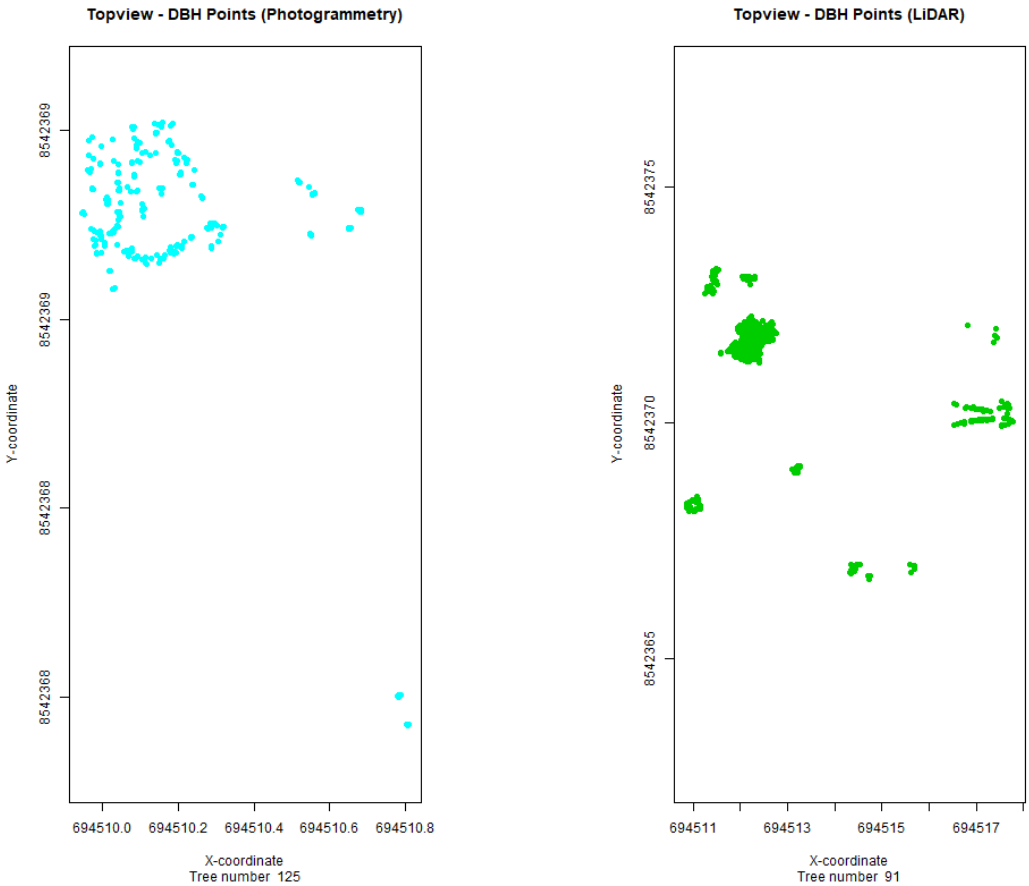

Figure 26 DBH Points of the same tree (left: photogrammetry, right: LiDAR)

The approach of finding the same trees in the two datasets using their mean coordinates resulted in 154 times the assumed same tree being found in both datasets. The mean distance between the center coordinates of trees is 2.14 meters, the minimum distance is 0.18 m, and the

maximum distance is 3.91 m. The fact that the offset between the trees is not constant is due to the tree segmentation algorithm and the resulting allocation and following determination of similar trees. In the LiDAR dataset more understory vegetation and smaller trees are assigned to higher trees, which can shift the center coordinates away from the actual coordinate of the tree. In the photogrammetry dataset it is the same with ground points. Further can the search radius chosen for the li2012 algorithm influenced the resulting dissected tree areas. This can be seen in the top view in Figure 24. In the next step the center coordinate of all points allocated to a tree id and respectively to a tree, are used to reference the trees between the two datasets and because the representation and allocation of other vegetation to a tree differ between the datasets, the offset between the trees is not constant, although the internal geometry is fine for both. This method bares some risk because due to the dense vegetation cover in the savanna woodland trees can wrongly be assigned to each other. Further can trees of the compared dataset be assigned multiple times, due to the use of two for-loops in the R script used to determine corresponding trees in the two datasets. The result of the script differs significant in the quality of the tree segmentation. In Figure 25 the better results of the tree segmentation and in Table 8 the key figures for these trees are shown. Figure 27 shows two examples where the script produced poor output for the tree segmentation. A proximity of the coordinates doesn't result in more accurate results in savanna area. It can be estimated that in an area with a more uniform vegetation cover the results of the tree segmentation and the following detection of identical trees will give better results.

Table 8 Examples results from the similar tree detection

Tree id (Photogrammetry)	Tree Id (LiDAR)	Offset in m	Height in m (Photogrammetry)	Crown Area in m² (Photogrammetry)	Height in m (LiDAR)	Crown Area in m² (LiDAR)
29	29	1.91	21.5	88.9	20.9	91.35
35	36	1.54	20.9	32.2	20.3	121.5
125	91	1	15.4	16.4	15.8	35.1
188	97	3.2	9.5	13.5	15.4	12.8

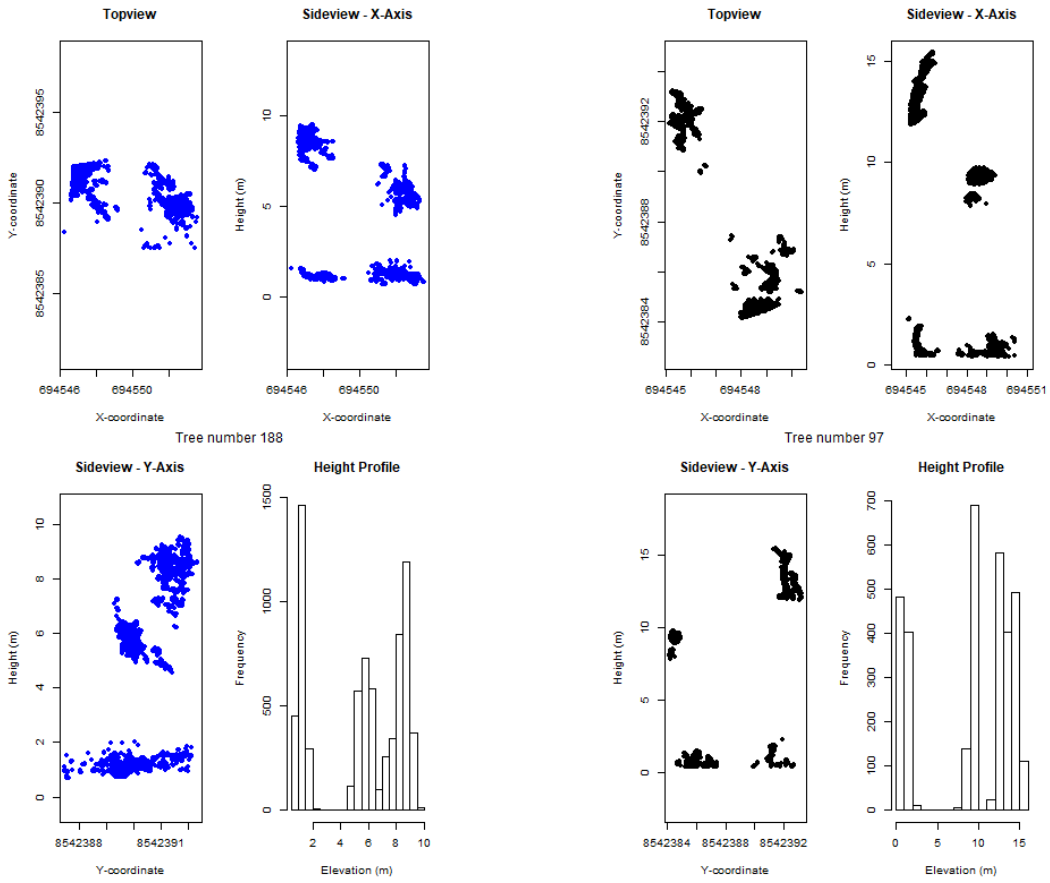

Figure 27 Poor results of the algorithms

4. General discussion

The results of the comparison of UAV-based LiDAR and photogrammetry show that there are differences between the two methods. The differences are due to flight planning, the methodology, and technical limitations.

4.1. Flight planning

The data used in this research was acquired in a flight with no discernible previous flight planning, which results in a random flight path. To achieve a certain quality of the LiDAR point cloud it is recommended to perform an initial flight path planning in preparation of the data acquisition with the target to set flight parameters as overlapping flight lines, varying flying speed and altitudes (Brede *et al.*, 2017). For the use of photogrammetry and SfM in forestry it is recommended to have overlapping images from multiple locations and angles to reduce occlusions and systematic errors and increase redundancy, further it is important that the objects for reconstruction are visible in multiple photos, for dense vegetation 6 photos, and it is

important to pay attention to factors as illumination and branch movement (Iglhaut *et al.*, 2019). In this research only the photos of one flight without prior flight planning was available as input data for the SfM algorithms. The second flight delivered unsuitable data because of the low sun position and the resulting distortion in the photos. As a result of the distortion in the pictures the SfM algorithm couldn't the photos.

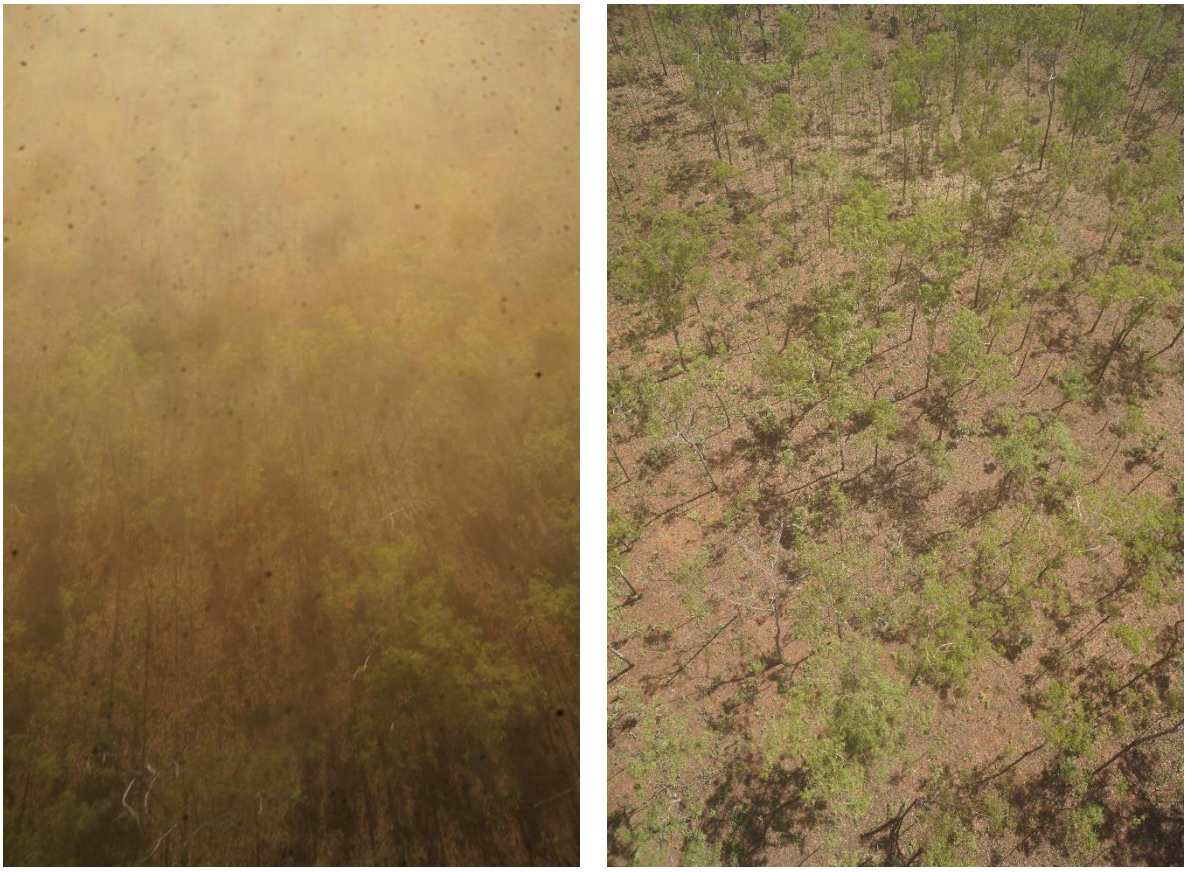

Figure 28 Picture acquired in flight 2 (left) and in flight 1 (right)

A further result of the missing flight plan is that in some parts of the photogrammetry point cloud the tree crowns are represented with a slight distortion compared to representation in the LiDAR point cloud. This result can occur, when a tree crown is only photographed from one side, because the SfM algorithm can calculate the point cloud of an object best, if photographs from all angels are available. An example for this is area in the north east corner of the research area, where the tree crowns are better represented in LiDAR dataset then in photogrammetry dataset. Overall it can be presumed that through a better flight planning and multiple flights with usable photos the results of the calculated photogrammetry point cloud would have been significantly better. For every use case the flight path and therefore the flight planning can

differ, so can the flight path for an optimal DSM be different from the required path for DTM construction.

4.2. Methodology

The Methodology can influence the results as well, the greatest variations can be observed in the calculation of the photogrammetry point cloud. During the process, some parameters in Agisoft PhotoScan can be chosen which have an impact of the resulting point cloud. The two main parameters which affect the quality of the result are ‘resolution’ and ‘depth filtering’.

In the first step of the photogrammetry workflow, the alignment of the photos, the most important parameter is the ‘accuracy’ parameter and has a large impact on the resulting sparse point cloud, because it upscales or downscales the used photos. The highest setting upscales the photo by 4, the setting ‘high’ uses the original size, and the low setting scales the photo down by 16. The results of the photo alignment can also be improved by adding the GPS coordinates and the angle of the cameras (Agisoft, 2018).

In the next step of the workflow the construction of the dense point cloud, the ‘quality’ and ‘depth filter’ parameters are most influential. The ‘quality’ parameter is similar to the accuracy parameter in the first step and responsible for the obtained detail and accurate geometry. The difference is that in ultra-high setting the original photos are used where the lower settings scale down the photo quality. The second important parameter here is depth filter, which uses filtering algorithms for outliers during the depth maps calculation, which can be caused by noise or a bad focus in the picture. The two extreme settings for this parameter are ‘mild’ and ‘aggressive’, ‘mild’ is recommended if small details are required which are spatially distinguished, whereas ‘aggressive’ sorts out most outliers and therefore is best suited for areas without important details. The third option for depth filtering is the option moderate where the results are between the two previous options (Agisoft, 2018).

These options are especially important for this research because the area of interest is savanna woodland and therefore highly accurate and detailed information is needed for the further steps taken in this project. The original approach was to use the highest possible accuracy and quality settings, in combination with the mild depth filter, due to time limitations as well as technical limitations cutbacks with the parameters were made towards the ‘high’ quality parameter (figure 5). The choice towards the ‘high’ quality parameter instead of the ‘ultra-high’ option may have consequences for the quality of the stem and tree crown reconstruction.

Further the choices for the parameters in the R script regarding the lastrees -function can influence the results. First the choice of the tree segmentation algorithm has an impact on the single tree detections and allocation of understory vegetation to trees. In this research only the li2012 algorithm was used, since all other algorithms need additional input data such as a CHM in addition to the point cloud.
The parameters for the li2012 algorithm have also a great influence on the result. The most significant parameters are the maximal crown size (SpeedUp) and the search radius (r).

4.3. Technical limitations

The calculations of point clouds with SfM algorithms requires high computational power, which can exceed the possibilities of today's common computer. Further points clouds can be big datasets, in sense of file size which can then complicate the data handling during the further calculations. In this research it was not possible to calculate the photogrammetry point cloud for the full captured area on high settings in Agisoft Photoscan due to insufficient memory. Also, the run time for building the dense point cloud can get extremely long, even with the network computing feature provided by the software. The calculation of the photogrammetry point cloud in this research for an extent of 300x300 m with 194 images took in average 3 days of run time and was therefore a limiting factor on the attempts on calculating the point cloud with different parameter settings.
Further the technical limitations had influence on the used resolution for the digital models. The chosen 0.5 m cell size was the highest resolution possible, limited by the LiDAR dataset, where the computer kept failing the cloud to cloud distance calculation in CloudCompare. To keep the digital model consistent all three calculated model were set to the resolution of 0.5 m cell size. The next step were the file size and the run time were noticeable was during the tree detection algorithms for the determination of the forest parameters. The run time for the LiDAR dataset was again longer then for the photogrammetry dataset, which is caused by the better representation of the trees in the dataset. For an extent of 100x100 m the run time of the tree detection algorithm was 2 ½ days. Therefore, it can be stated that the extent of the area of interest and the chosen quality can lead to technical limitations. For this research, the crop down of the extent to 100x100 m didn't limit the possibility to answer the research questions. This might not be the case for every use case.

4.4. Evaluation of the Results

The results obtained for the DTM's showed that there is potential for the application of SfM photogrammetric applications in sparse vegetation areas as savannas. The vegetation cover however is the most limiting factor for photogrammetry due to limitations in penetrating vegetation cover (Wallace *et al.*, 2016). Whereas in urban areas the photogrammetry derived DTM's are as accurate as the LiDAR derived (Polat and Uysal, 2018), for highly vegetated areas with broken terrain photogrammetry DTM's are losing accuracy (Akturk and Altunel, 2019).

Further the results of this study show that the photogrammetry derived DSM and CHM show good quality results compared to LiDAR derived models. This fits to the results of studies as Herrero-Huerta et al., (2016) which used the integration of photogrammetry derived point cloud data with LiDAR data to construct a dense canopy height model. Also, Iglhaut et al. (2019), mentions the lack of high accuracy DTM's to normalize the photogrammetry point cloud as one of the main challenges of this technique. These studies imply that advantage of photogrammetry is in the representation of the canopy cover, which is also the case in this research. The lower quality of the photogrammetry DTM compared to the LiDAR DTM leads to the difference of 4,5 m between the minimum elevation values of the LiDAR and photogrammetry CHM. It should be noted that these studies relate to densely forested areas, compared to the sparser forested savanna woodland.

Further the results of this study are similar to the results of Wallace et al. (2016), who compared LiDAR and photogrammetry for a dry eucalypt forest. Their study showed less canopy cover for photogrammetry and better estimates for vertical structure of individual trees with LiDAR. The calculated canopy cover is here higher for the photogrammetry (82%) then for the LiDAR (80%), which contrasts the results of Wallace et al. (2016), where for photogrammetry 50% canopy cover was predicted and for LiDAR 63%. On the other hand, the results of this study regarding the estimated vertical structure of individual trees can be compared to the results of Wallace. Regarding the individual tree detection Wallace et al. (2016) got the different results as this study. In the study of Wallace et al. (2016) in the photogrammetry dataset were 50 % less trees detected compared to the LiDAR dataset. In this research on the contrary more trees were detected in the photogrammetry dataset (209) than in the LiDAR data (189).

Goldbergs et al. (2018) study showed also that the capture of mid story and understory vegetation structure is better covered by LiDAR data then compared to photogrammetry. Further the study showed better results regarding the quality of the photogrammetry derived

DTM compared to their LiDAR counterpart. In the study by Goldbergs et al. (2018) the mean error of difference between LiDAR and photogrammetry was 0.08 m compared to – 0.71 m in this study.

This study backs up the results of Wallace et al. (2016), that UAV-based photogrammetry can be used as a low cost alternative to LiDAR technique for surveying forest stands and that both techniques can be used to monitor savanna woodlands. Further, it shows that the point cloud calculated with photogrammetry can be used as input in tree segmentation algorithms and the results are of similar quality as the LiDAR results. Further this research indicates that it is not yet possible to calculate the diameter at breast height in an automated way. It shows that determination of forest parameters is possible with the use of tree segmentation algorithms. However, the detection of mid- and understory trees is still a problem for the algorithm in both the LiDAR and the photogrammetry point clouds.

5. Conclusion

This research compared the two remote sensing technique LiDAR and SfM photogrammetry in order to determine whether SfM photogrammetry can be used as an alternative to LiDAR for monitoring savanna ecosystems. This was done by assessing standard geographical elevation models derived from the remote sensing techniques and second the comparison of forest parameters as tree count, canopy area, and DBH. The research questions and their brief answers will follow below.

It was possible to calculate all digital models which is a promising aspect of the research and motivates for further research into this topic. The results are depending as expected on the input data, which are needed in a certain quality to produce results which can be used as an alternative to LiDAR.

The result of the comparison of the digital models found that photogrammetry can be used as an alternative to LiDAR. The DTM derived from photogrammetry can be used as an alternative to the LiDAR derived DTM when the use case is estimating forest parameters, because the mean difference between photogrammetry and LiDAR is -0.69 m. For the DSM and CHM, the results are good enough to justify photogrammetry as an alternative to LiDAR. The mean differences between the LiDAR and the photogrammetry derived digital models is for the DSM -0.56 m and 0.12 m for the CHM. The usability of the photogrammetry models as an alternative to the LiDAR models, is depended on the use case and the therefore chosen parameter settings.

It was possible to calculate the tree count, the canopy area in m^2 as well as the gap area in m^2. The tree count algorithm in the photogrammetry dataset detected more trees than were detected in the compared LiDAR dataset. Also, the differences in the canopy cover are just minor, 80% (LiDAR) compared to 82% (photogrammetry) covered area. The mean crown area per tree is also comparable for the results of the two methods, in the LiDAR dataset the mean crown size is 42.2 m² compared to 42.5 m² in the photogrammetry dataset. For neither of the two datasets was it possible to estimate the DBH, which is therefore the only parameter which couldn't be calculated for both datasets. The mean tree height differs only by 1 m, which is consistent with the slight differences between the dataset's other parameters.

The SfM technique is a promising approach for a lower cost alternative to LiDAR in regard to the monitoring certain parts of savanna woodland, as for example dominant trees (Wallace et al., 2016, Goldbergs et al., 2018). In this study the results of photogrammetry data are of comparable quality to the LiDAR data and therefore is SfM photogrammetry found to be an alternative to the more expensive LiDAR technique for the determination of forest parameters in savanna woodlands. The results are suggesting that both techniques can be used to monitor the land use change in savanna ecosystems, because it is possible to monitor the composition of dominant, understory trees, shrubs and grass areas.

References

Ackermann, F. (1999) *Airborne laser scanning-present status and future expectations*, *ISPRS Journal of Photogrammetry & Remote Sensing*. Available at: https://ac.els-cdn.com/S092427169900009X/1-s2.0-S092427169900009X-main.pdf?_tid=93f78164-d051-4e4f-9dc2-40aa42215475&acdnat=1552659940_3364a7f0d4b106aa5f5e592fce2586aa (Accessed: 15 March 2019).

Agisoft (2018) *Agisoft PhotoScan User Manual Professional Edition, Version 1.4*. Available at: https://www.agisoft.com/pdf/photoscan-pro_1_4_en.pdf (Accessed: 7 January 2019).

Akturk, E. and Altunel, A. O. (2019) 'Accuracy assessment of a low-cost UAV derived digital elevation model (DEM) in a highly broken and vegetated terrain', *Measurement*. Elsevier, 136, pp. 382–386. doi: 10.1016/J.MEASUREMENT.2018.12.101.

Alam, S. A. and Starr, M. (2013) 'Impacts of climate change on savannah woodland biomass carbon density and water-use: a modelling study of the Sudanese gum belt region', *Mitigation and Adaptation Strategies for Global Change*. Springer Netherlands, 18(7), pp. 979–999. doi: 10.1007/s11027-012-9403-5.

Awange, J. (2018) *GNSS Environmental Sensing*. doi: 10.1007/978-3-319-58418-8.

Bodini, A. and Clerici, N. (2016) 'Vegetation, herbivores and fires in savanna ecosystems: A network perspective', *Ecological Complexity*. Elsevier, 28, pp. 36–46. doi: 10.1016/J.ECOCOM.2016.10.001.

Brede, B. *et al.* (2017) 'Comparing RIEGL RiCOPTER UAV LiDAR Derived Canopy Height and DBH with Terrestrial LiDAR'. doi: 10.3390/s17102371.

Chen, C. *et al.* (2018) 'A Robust Algorithm for Constructing Pit-Free Canopy Height Model', *Journal of the Indian Society of Remote Sensing*. Springer India, 46(4), pp. 491–499. doi: 10.1007/s12524-017-0710-x.

Chen, X., Hutley, L. B. and Eamus, D. (2003) 'Carbon balance of a tropical savanna of northern Australia', *Oecologia*. Springer-Verlag, 137(3), pp. 405–416. doi: 10.1007/s00442-003-1358-5.

Ford, A. T., Fryxell, J. M. and Sinclair, A. R. E. (2016) 'Conservation Challenges Facing African Savanna Ecosystems', in *Antelope Conservation*. Chichester, UK: John Wiley & Sons, Ltd, pp. 11–31. doi: 10.1002/9781118409572.ch2.

Fritz, A., Kattenborn, T. and Koch, B. (2013) 'UAV-BASED PHOTOGRAMMETRIC POINT CLOUDS - TREE STEM MAPPING IN OPEN STANDS IN COMPARISON TO TERRESTRIAL LASER SCANNER POINT CLOUDS', *International Archives of the Photogrammetry, Remote Sensing and Spatial Information Science*, XL-1/W2(2013), pp. 141–146. doi: 10.1039/c6nr02690g.

Goldbergs, G. *et al.* (2018) 'Efficiency of Individual Tree Detection Approaches Based on Light-Weight and Low-Cost UAS Imagery in Australian Savannas', *Remote Sensing*. Multidisciplinary Digital Publishing Institute, 10(2), p. 161. doi: 10.3390/rs10020161.

Goshtasby, A. A. (2012) *Image Registration*. Springer London Dordrecht Heidelberg New York.

Gupta, R. P. (2018) 'Digital Elevation Model', in *Remote Sensing Geology*. Berlin, Heidelberg: Springer Berlin Heidelberg, pp. 101–106. doi: 10.1007/978-3-662-55876-8_8.

Gwenzi, D. and Lefsky, M. A. (2014) 'Modeling canopy height in a savanna ecosystem using spaceborne lidar waveforms', *Remote Sensing of Environment*, 154, pp. 338–344. doi: 10.1016/j.rse.2013.11.024.

Herrero-Huerta, M. *et al.* (2016) 'Dense Canopy Height Model from a low-cost photogrammetric platform and LiDAR data', *Trees*. Springer Berlin Heidelberg, 30(4), pp. 1287–1301. doi:

10.1007/s00468-016-1366-9.

Iglhaut, J. *et al.* (2019) 'Structure from Motion Photogrammetry in Forestry: a Review', *Current Forestry Reports*. Springer International Publishing, 5(3), pp. 155–168. doi: 10.1007/s40725-019-00094-3.

Karan, M. *et al.* (2016) 'The Australian SuperSite Network: A continental, long-term terrestrial ecosystem observatory', *Science of The Total Environment*. Elsevier, 568, pp. 1263–1274. doi: 10.1016/J.SCITOTENV.2016.05.170.

Lemmens, M. (2011a) 'Airborne Lidar', in *Geo-information*. Dordrecht: Springer Netherlands, pp. 153–170. doi: 10.1007/978-94-007-1667-4_8.

Lemmens, M. (2011b) 'Photogrammetry: Geometric Data from Imagery', in *Geo-information Technologies, Applications and the Environment*. Dordrecht: Springer Netherlands, pp. 123–151. doi: 10.1007/978-94-007-1667-4_7.

Linder, W. (2009) *Digital Photogrammetry*. 3rd edn. Heidelberg: Springer Berlin Heidelberg. doi: 10.1007/978-3-540-92725-9.

Polat, N. and Uysal, M. (2018) 'An Experimental Analysis of Digital Elevation Models Generated with Lidar Data and UAV Photogrammetry', *Journal of the Indian Society of Remote Sensing*. Springer India, 46(7), pp. 1135–1142. doi: 10.1007/s12524-018-0760-8.

RIEGL (no date) *RIEGL - RIEGL Laser Measurement Systems*. Available at: http://www.riegl.com/fileadmin/gallery/UAS_UAV/uls_ricopter_quarry.jpg (Accessed: 19 March 2019).

Sankaran, M. *et al.* (2005) 'Determinants of woody cover in African savannas', *Nature*. Nature Publishing Group, 438(7069), pp. 846–849. doi: 10.1038/nature04070.

Sivkumar, M. (2007) 'Interactions between climate and desertification', *Agricultural and Forest Meteorology*. Elsevier, 142(2–4), pp. 143–155. doi: 10.1016/J.AGRFORMET.2006.03.025.

Skarpe, C. (1992) 'Dynamics of savanna ecosystems', *Journal of Vegetation Science*, 3(3), pp. 293–300. doi: 10.2307/3235754.

Southworth, J. *et al.* (2016) 'Changes in vegetation persistence across global savanna landscapes', *Journal of Land Use Science*, 11(1), pp. 7–32. doi: 10.1080/1747423X.2015.1071439.

TERN (no date) *SuperSites - What is a SuperSite?* Available at: https://supersites.tern.org.au/about-us/what-is-a-supersite (Accessed: 7 January 2019).

Wallace, L. *et al.* (2016) 'Assessment of Forest Structure Using Two UAV Techniques: A Comparison of Airborne Laser Scanning and Structure from Motion (SfM) Point Clouds', *Forests*. Multidisciplinary Digital Publishing Institute, 7(12), p. 62. doi: 10.3390/f7030062.

Wandinger, U. (2005) 'Introduction to Lidar', in *Lidar*. New York: Springer-Verlag, pp. 1–18. doi: 10.1007/0-387-25101-4_1.

Westoby, M. J. *et al.* (2012) '"Structure-from-Motion" photogrammetry: A low-cost, effective tool for geoscience applications', *Geomorphology*. Elsevier B.V., 179, pp. 300–314. doi: 10.1016/j.geomorph.2012.08.021.

Appendices

Appendix A: tree_detection script

```
library(sp)
library(rgl)
library(raster)
library(lidR)
library(colorRamps)

setwd("E:/Masterarbeit/Data/LidR_data")

LiDARfile <- "input/classify_l2las.laz"
PHOTOfile <- "input/classify_p2las.laz"

lidar= readLAS(LiDARfile)
photo= readLAS(PHOTOfile)

epsg(lidar)= 32752
epsg(photo)= 32752

DTM_lidar <- grid_terrain(lidar, res=0.5, algorithm = knnidw(k=6L, p = 2), keep_lowest = FALSE)
DTM_photo <- grid_terrain(photo, res=0.5, algorithm = knnidw(k=6L, p = 2), keep_lowest = FALSE)

nlidar <- lasnormalize(lidar,DTM_lidar)
nphoto <- lasnormalize(photo,DTM_photo)

Vegpoints_norm_lidar <- nlidar %>% lasfilter(Classification==5)
Vegpoints_norm_photo <- nphoto %>% lasfilter(Classification==5)

trees_l <- lastrees(Vegpoints_norm_lidar, li2012(R=5, speed_up=7.5, hmin=5))
trees_p <- lastrees(Vegpoints_norm_photo, li2012(R=5, speed_up=7.5, hmin=5))

(max(trees_l@data$treeID, na.rm=TRUE))
(max(trees_p@data$treeID, na.rm=TRUE))

dir.create( "results_detection_photo")

d_l=NULL

for (i in 1:max(trees_l@data$treeID, na.rm=TRUE)){
  print(i)
  tree <- trees_l %>% lasfilter(treeID==i, Classification==5)
  height <- max(tree@data$Z)
  meanx <- mean(tree@data$X)
  meanY <- mean(tree@data$Y)
  int <- mean(tree@data$Intensity)
  count <- as.numeric(length(tree@data$Z))

  canopy <- tree %>% lasfilter(Z>5)
  X <- as.vector(canopy@data$X)
  Y <- as.vector(canopy@data$Y)
```

```
 XY<- cbind(X,Y)
 hpts<-chull(XY)
 hpts<- c(hpts, hpts[1])
 crown.coords <- XY[hpts,]
 crown.poly <- Polygon(crown.coords, hole=F)
 crown.area <- crown.poly@area

 PCA <- prcomp(XY, scale=F)
 PCA.ev.ratio <- PCA$sdev[1]/PCA$sdev[2]
 score <- ifelse(PCA.ev.ratio>1.2,0,1)

 d_l = rbind(d_l, data.frame(i,meanx,meanY, height, crown.area,PCA.ev.ratio, score, count))

 png(paste("results_detection/tree", i, ".png"), height=800, width=400)
 par(mfrow=c(2,2))
 plot(tree@data$Y~tree@data$X, asp=1, pch=19, col= tree@data$NumberOfReturns,
main="Topview - NumberOfReturns", xlab="X-coordinate", ylab="Y-coordinate")
 plot(tree@data$Z~tree@data$X, asp=1, pch=19, col=tree@data$ReturnNumber, main ="Sideview -
Returnnumber", xlab="X-coordinate", ylab="Height (m)")
 plot(tree@data$Z~tree@data$Y, asp=1, pch=19, col=tree@data$Classification, main="Sideview -
Classification", xlab="Y-coordinate", ylab="Height (m)")
 hist(tree@data$Z, main="Height Profile", xlab="Elevation (m)")
 dev.off()
}

d_p=NULL

for (i in 1:max(trees_p@data$treeID, na.rm=TRUE)){
 print(i)
 tree <- trees_p %>% lasfilter(treeID==i, Classification==5)
 height <- max(tree@data$Z)
 meanx <- mean(tree@data$X)
 meanY <- mean(tree@data$Y)
 int <- mean(tree@data$Intensity)
 count <- as.numeric(length(tree@data$Z))

 canopy <- tree %>% lasfilter(Z>5)
 X <- as.vector(canopy@data$X)
 Y <- as.vector(canopy@data$Y)
 XY<- cbind(X,Y)
 hpts<-chull(XY)
 hpts<- c(hpts, hpts[1])
 crown.coords <- XY[hpts,]
 crown.poly <- Polygon(crown.coords, hole=F)
 crown.area <- crown.poly@area

 PCA <- prcomp(XY, scale=F)
 PCA.ev.ratio <- PCA$sdev[1]/PCA$sdev[2]
 score <- ifelse(PCA.ev.ratio>1.2,0,1)

 d_p = rbind(d_p, data.frame(i,meanx,meanY, height, crown.area,PCA.ev.ratio, score, count))
```

```
  png(paste("extracted_trees_Vegpoints_urban/tree", i, ".png"), height=800, width=400)
  par(mfrow=c(2,2))
  plot(tree@data$Y~tree@data$X, asp=1, pch=19, col= tree@data$NumberOfReturns,
main="Topview - NumberOfReturns", xlab="X-coordinate", ylab="Y-coordinate")
  plot(tree@data$Z~tree@data$X, asp=1, pch=19, col=tree@data$ReturnNumber, main ="Sideview -
Returnnumber", xlab="X-coordinate", ylab="Height (m)")
  plot(tree@data$Z~tree@data$Y, asp=1, pch=19, col=tree@data$Classification, main="Sideview -
Classification", xlab="Y-coordinate", ylab="Height (m)")
  hist(tree@data$Z, main="Height Profile", xlab="Elevation (m)")
  mtext(paste("Tree number",i), side = 3, line = -34 ,outer = TRUE)
  dev.off()
}

write.csv(d_l,file = "results_detection/trees_lidar.csv" )
write.csv(d_p,file = "results_detection_photo/trees_photo.csv" )
```

Appendix B: detection_DBH_points script

```
library(sp)
library(rgl)
library(raster)
library(lidR)
library(colorRamps)

for (i in 1:max(trees_p@data$treeID, na.rm=TRUE)){
  print(i)
  tree <- trees_p %>% lasfilter(treeID==i, Classification==5)
  DBH_points <- tree %>% lasfilter(Z>1.30 & Z<1.5)

  if(is.empty(DBH_points)){
    next()
  }else{
  png(paste("Photo_DBH_Points_tree", i, ".png"), height=800, width=400)
  plot(DBH_points@data$Y~DBH_points@data$X, asp=1, pch=19, col=
DBH_points@data$NumberOfReturns, main="Topview - DBH Points (Photogrammetry)", xlab="X-
coordinate", ylab="Y-coordinate", sub=paste("Tree number ",i))
  dev.off()
  }
}
```

Appendix C: Finding_similar_trees script

```
library(sp)
library(rgl)
library(raster)
library(lidR)
library(colorRamps)


d_test = NULL

for (i in 1:max(trees_p@data$treeID, na.rm=TRUE)){
  print(i)
  tree <- trees_p %>% lasfilter(treeID==i, Classification==5)
  meanxP <- mean(tree@data$X)
  meanYP <- mean(tree@data$Y)
  Count_Photo <- i
  for (i in 1:max(trees_l@data$treeID, na.rm=TRUE)){
    Count_LiDAT <- i
    tree1 <- trees_l %>% lasfilter(treeID==i, Classification==5)
    meanxL <- mean(tree1@data$X)
    meanYL <- mean(tree1@data$Y)
    obergrenzex <- meanxL+3
    obergrenzey <- meanYL+3
    untergrenzex <- meanxL-3
    untergrenzey <- meanYL-3

    if(meanxP < obergrenzex & meanxP > untergrenzex){
      if(meanYP < obergrenzey & meanYP > untergrenzey){
        dx <- meanxL- meanxP
        dy <- meanYL- meanYP
        os <- sqrt((meanxP - meanxL)^2+(meanYP - meanYL)^2)
        d_test = rbind(d_test,data.frame(Count_Photo,Count_LiDAT,dx,dy,os))
        break()
      }else{
        next()
      }
    }
  }

}

write.csv(d_test,file = "Bäume_similarCoordinates.csv" )
```